Chapter

Evolution of Microwave Electric Field on Power Coupling to Plasma during Ignition Phase

Chinmoy Mallick, Mainak Bandyopadhyay and Rajesh Kumar

Abstract

During the gas ignition process, the plasma and the microwave electric fields are evolved with time together in the plasma volume. The spatio-temporal evolution pattern of microwave-radiated plasma parameters is reported here, highlighting the role of these electric fields on power coupling processes. Evolutions of electric field and so power coupling processes are calculated using the finite element method (FEM). It is observed that the main power coupling mechanism is electron cyclotron resonance (ECR) method; however, with the evolution of plasma, the mode shifts from ECR to off-ECR-type heating with time. Off-ECR heating in the form of upper hybrid resonance (UHR) method, electrostatic (ES) ion acoustic wave heating method is important heating mechanisms during highly dense plasma condition, when density is above critical density for launched frequency, 2.45 GHz. The conclusions on the shifting of heating mechanisms are also drawn based on the 3D maps of spatio-temporal plasma density and hot electron temperature evolution.

Keywords: microwave plasma simulation, COMSOL multi-physics, magnetized plasma evolution, ECR, off-resonance, ion source, electrostatic heating, electric field evolution, hot electron temperature, experimental validation

1. Introduction

Gaseous particles are ionized to bring them in the form of plasma through the various heating techniques. One of the popular heating techniques is the injection of high frequency microwaves (MW) to a cylindrical cavity that has comparable dimension to the injected MW wavelength. The MW plasma generated by the continuous or pulse feeding of the MW is used in the applications of industrial and accelerator fields for the material science and nuclear applications, respectively. In both of the feeding cases, the plasma is basically produced due to the power absorption by the electrons from the space-time dependent electric field of the MW. The spatio-temporal dynamics and also the steady-state behaviors of the plasma are governed by the ways the MW are coupled to the plasma sustained inside a cavity. The behavioral pattern of the electric field during the plasma evolution can help us to comment on the different MW coupling ways/mechanisms that are involved in the formation of plasma particles and their confinement scenarios. By mastering the basic concepts on those different coupling mechanisms, the coupling efficiency and so the performance of that particular plasma source can be optimized. Performance

optimization for this kind of plasma source is indispensable as these are involved in various kinds of applications as mentioned above. One of the important plasma devices is the microwave ion sources that are operated in continuous as well as pulse mode to extract the ion beam during the transient and steady state periods of plasma loading conditions [1–5]. The beam qualities are influenced by the MW coupling mechanisms as they are involved in deciding the plasma parameters during the extraction of a particular instant of the plasma evolution time. Several studies have already reported the electric field evolution during few 10 s of microsecond range when the plasma density was increasing in the very similar plasma device. The electric field was dropped by about more than 50% within a span of few microseconds after the MW launch (t = 0 s) into the cavity [6–11].

Since the electric fields can affect the different power coupling mechanisms during the gas ignition moment (ns to μs), the spatio-temporal plasma parameters are influenced significantly especially in the low pressure regime. Many researchers have used the kinetic models like PIC/MCC or even the hybrid fluid/PIC to obtain more precise results in the MW plasma discharge. But they failed to estimate the hot electron dynamics efficiently in lower pressure condition, as these models demand intensive computational hardware due to its particle approach. Therefore, the current chapter presents the electric field evolution and its impact on the plasma parameter build-up during low pressure plasma state. Here, the model used is based on the finite element method (FEM) that gives more appropriate results for the transient plasma parameters through fluid modeling approach and time-dependent, partial differential equation solver (TDPDE) using fewer computer resources [11]. The different MW-plasma coupling mechanisms (ECR, UHR and electric field polarity reversal associated with ES wave heating) during the plasma density evolution after the MW launch (t = 0 s) can be understood from the behaviors of electric fields.

2. Basic theory of microwave plasma interaction

The study on the propagation and interactions of the microwave with the plasma is important to optimize the performance of any plasma devices like the microwave ion sources. The microwave propagation in the plasma is affected by the dielectric prosperities of the plasma medium. The dielectric property, i.e., the permittivity or the refractive index of the plasma, depends on the external magnetic field distribution that is used to confine the plasma particles and also the electrostatic fields that are present in the plasma. Therefore, the microwave while propagating in different directions within the plasma encounters different values of the refractive index as well as the permittivity that makes the magnetized plasma to be anisotropic and inhomogeneous, respectively. To generate a high plasma density, which is one of the primary requirements in some microwave plasma devices, viz., the microwave discharge ion source (MDIS) or electron cyclotron resonance ion sources (ECRIS), an optimum coupling of the microwave energy through the different interaction mechanisms to the plasma medium is necessary. The microwave propagation and the coupling mechanisms are also influenced by the boundary conditions present in the plasma devices and the geometrical shape of the plasma device. In most cases, the dimension of the plasma reactor used for the purpose of ion sources lie in the comparable range of the launched microwave wavelength. This means the microwave electromagnetic field propagation within the ion source reactor (or cavity) is guided by the boundary conditions and the geometrical shape of the ion source cavity. So, the microwave electromagnetic field coupling to the plasma is affected if the cavity geometry is perturbed. Due to the modification of the cavity geometry, the resonating properties of the cavity resonator are no longer dominated by the

fundamental cavity resonant mode. The cavity can resonate with some additional resonating frequencies including the fundamental one. The additional resonating frequencies can lie near to the fundamental one. Due to this reason, if the microwave is launched to the modified cavity, the total microwave field is shared among the cavity resonant modes including the fundamental one and contributes to the power coupling to the plasma.

From the electromagnetic theory of a resonant cavity, only particular cavity resonant modes can exist having fixed frequencies that are given by [12, 13]

$$f = \frac{1}{2\pi}\sqrt{\frac{r^2\pi^2}{l^2} + h^2} \tag{1}$$

where r, l and h are the integer, the length of the plasma cavity and the eigenvalues of the cavity, respectively. The eigenvalues are obtained from the solution of the equations gives by:

$$\nabla_t^2 H_{z0} + h^2 H_{z0} = 0 \tag{2}$$

$$\nabla_t^2 E_{z0} + h^2 E_{z0} \tag{3}$$

A theoretical calculation for the cavity resonant modes from the eigenvalue equations for the electromagnetic field [12, 13] is performed from the empty and completely closed cavity. By considering a simplest cylindrical cavity of radius r and the length 'd' that is filled with a dielectric constant ε_r and the relative permittivity μ_r, the resonant frequencies allowed by the cavity that can be determined from the eigenvalue equations are shown below from the TE and TM modes:

$$f_{nml}^{TE} = \frac{c}{2\pi\sqrt{\mu_r\varepsilon_r}}\sqrt{\left(\frac{P'_{nm}}{r}\right)^2 + \left(\frac{l\pi}{d}\right)^2} \tag{4}$$

$$f_{nml}^{TE} = \frac{c}{2\pi\sqrt{\mu_r\varepsilon_r}}\sqrt{\left(\frac{P_{nm}}{r}\right)^2 + \left(\frac{l\pi}{d}\right)^2} \tag{5}$$

Here, P_{nm} and P'_{nm} are, respectively, the zeros of order m of the Bessel functions of order n and its first derivative. The indices represent the three-dimensional electromagnetic field patterns for each cavity resonant mode.

2.1 Microwave propagation in plasmas

In case of magnetized plasma, the microwave propagation is influenced by the plasma particle dynamics. As the plasma particle dynamics are represented by the particle velocity, the thermal velocity of the plasma particles should be considered when the microwave propagation in plasma is discussed. If the thermal velocity of the plasma particles is negligible with respect to the phase velocity of the microwave, i.e., $v_{thermal} \ll v_{phase}$, this approximation is useful for determining the dispersion of the microwave in a magnetized plasma. This approximation also known as 'cold plasma' is not applicable to the locations where the microwave encounters resonance in the magnetized plasma. On the other hand, if the temperature of the plasma particles is high enough that makes the velocity of the particle to be relativistic (also called as 'warm plasma'), the influence of the plasma particles cannot be neglected while determining the microwave propagation. In that case, the damping of the microwave field is greatly influenced by the plasma particles.

For the un-magnetized plasma case in which the plasma is considered to be isotropic and the condition, $v_{thermal} \ll v_{phase}$ is satisfied, the plasma fluid equation is written as:

$$\frac{\partial \tilde{v}}{\partial t} = q\tilde{E} \tag{6}$$

If the microwave electric field ($\tilde{E}$) and the velocity ($\tilde{v}$) are assumed to be varying with $e^{i\omega t}$, the plasma dielectric constant can be easily shown as:

$$\epsilon = \epsilon_0 \left(1 - \frac{\omega_{pe}^2}{\omega^2}\right) \tag{7}$$

where the ω_{pe} is the electron plasma frequency that is also obtained from the electron density by the relation:

$$\omega_{pe} = \sqrt{\frac{n_e e^2}{\epsilon_0 m_e}} \tag{8}$$

where m_e, e and ϵ_0 are the electron mass, charge and electrical permittivity in vacuum condition, respectively. So the electrical permittivity in plasma is affected by the plasma density. As the electrical permittivity has to be positive in ideal case, the plasma density has to be lower than the corresponding microwave frequency that is launched externally to energize the plasma particles. Therefore, in case of homogeneous and isotropic plasma, it is not possible to raise the plasma density beyond certain level that is known as the critical density, which is written as $n_{critical} = \omega_{pe}^2 \left(\frac{\epsilon_0 m_e}{n_e e^2}\right)$. The density below and above the critical density is referred to be underdense and overdense plasma. So the critical density is the main limitation in the un-magnetized plasma for the microwave propagation. The dispersion for the wave in magnetized plasma is written as:

$$\omega^2 - \omega_{pe}^2 = k^2 c^2 \tag{9}$$

In the overdense plasma, if $\omega < \omega_{pe}$, the propagation k-vector $'k'$ becomes imaginary that means the complete reflection of the incoming microwave from the plasma. Therefore, if the microwave propagation is assumed to be propagating in the x-direction in the overdense plasma, the electric field of the microwave can be written as:

$$\tilde{E} = \tilde{E}_0 e^{(ik.\tilde{r} - \omega t)} = \tilde{E}_0 e^{(ikx - \omega t)} = e^{\frac{x}{\delta}} e^{-i\omega t} \tag{10}$$

So, before encountering the overdense plasma, the electric field becomes an evanescent wave as its magnitude decays exponentially within a distance of approximately the skin depth value; $(\delta) = c/\left(\sqrt{\omega_{pe}^2 - \omega^2}\right)$.

Under the externally applied magnetic field, the dielectric constant for the anisotropic plasma becomes a tensor quantity. It means the microwave propagation becomes dependent on the plasma dielectric properties while propagating in various directions with respect to the externally applied magnetic field. If the magnetic field is oriented axially ($\tilde{B} = B_0\tilde{z}$) in a cylindrical plasma chamber, the plasma can act as a dielectric with current $\tilde{J}$ and also the Maxwell's equations can be rewritten as:

$$\tilde{\nabla} \times \tilde{B} = \mu_0 \left(\tilde{J} + \varepsilon_0 \frac{\partial \tilde{E}}{\partial t} \right) = \mu_0 \frac{\partial \tilde{D}}{\partial t} \tag{11}$$

Now if the plasma motion follows the $e^{i\omega t}$ dependence and the plasma conductivity tensor is related with the current as $\bar{\bar{\sigma}}.\,\tilde{E} = \tilde{J}$, the relation between $\tilde{D}$ and $\tilde{E}$ is obtained as:

$$\tilde{D} = \varepsilon_0 \left(\bar{\bar{I}} + \frac{i}{\varepsilon_0 \omega} \bar{\bar{\sigma}} \right) \tilde{E} \tag{12}$$

where the symbol $\bar{\bar{I}}$ represents an identity tensor. In short, the parameter $\tilde{D}$ can also be written as $\tilde{D} = \varepsilon_0 \, \bar{\bar{\epsilon}}_r \, \tilde{E}$, where the effective dielectric tensor $\bar{\bar{\epsilon}}$ is represented as $\epsilon_0 \left(\bar{\bar{I}} + \frac{i}{\varepsilon_0 \omega} \bar{\bar{\sigma}} \right)$. The plasma conductivity tensor is evaluated from the fluid plasma approach. Therefore, the fluid equation in case of 'cold plasma' approximation is rewritten by neglecting the collisional and pressure term and the magnetic field term is considered as:

$$m_i \frac{\partial \tilde{v}}{\partial t} = e\left(\tilde{E} + \tilde{v} \times \tilde{B} \right) \tag{13}$$

The solution to this equation brings out the relation between the velocity ($\tilde{v}$) and the electric field of the microwave. As $\tilde{J} = ne\tilde{v}$, the final expression for the effective dielectric tensor $\bar{\bar{\epsilon}}$ can be shown in a determinant form as:

$$\bar{\bar{\epsilon}} = \epsilon_0 \begin{vmatrix} S & -iD & 0 \\ iD & S & 0 \\ 0 & 0 & P \end{vmatrix} \equiv \epsilon_0 \, \bar{\bar{\epsilon}}_r \tag{14}$$

where S, D and P can be written in terms of three different kinds of frequencies: $S = \left[1 - \frac{\omega_{pe}^2}{\omega^2} \left(\frac{1}{1-\omega_c} \right) \right]$, $D = \left[- \frac{\omega_{pe}^2}{\omega^2} \frac{\omega_c}{\omega} \left(\frac{1}{1-\omega_c} \right) \right]$ and $P = 1 - \frac{\omega_{pe}^2}{\omega^2}$.

The wave equation can be derived from the Maxwell's curl equation for the electric field by following the standard procedure that shows

$$\tilde{\nabla} \times \tilde{\nabla} \times \tilde{E} = - \frac{\partial \tilde{\nabla} \times \tilde{B}}{\partial t} = - \frac{1}{c^2} \bar{\bar{\epsilon}} \, . \frac{\partial^2 \tilde{E}}{\partial t^2} \tag{15}$$

The above equation is rewritten by assuming the $e^{i\tilde{k}.\tilde{r}}$ dependence of the electric field as:

$$\tilde{k} \times \tilde{k} \times \tilde{E} + \frac{\omega^2}{c^2} \bar{\bar{\epsilon}} \, . \tilde{E} = 0 \tag{16}$$

The equation can be represented in matrix form by assuming the angle between the wave vector and magnetic field to be 'θ' and denoting the vector $\tilde{N} = \frac{c}{\omega} \tilde{k}$.

$$\begin{bmatrix} S - N^2 cos^2\theta & -iD & N^2 cos\theta sin\theta \\ iD & S - N^2 & 0 \\ N^2 cos\theta sin\theta & 0 & P - N^2 sin^2\theta \end{bmatrix} \begin{bmatrix} E_x \\ E_y \\ E_z \end{bmatrix} = 0 \tag{17}$$

The solution to these equations can exist if the determinant is zero. This condition brings out the dispersion relation of the microwave in the plasma. By making the determinant to be zero, two solutions are obtained that are written as:

$$N_{O,X}^2 = \frac{2x(1-x)}{2(1-x) - y^2 sin^2\theta \pm \sqrt{y^4 sin^4\theta \pm 4y^2(1-x)^2 cos^2\theta}} \tag{18}$$

where the symbols '*O*' and '*X*' correspond to the ordinary microwave and extraordinary microwave, respectively. The notations x and y in Eq. (18) represent the electron density scale and magnetic field scale respectively and are denoted as: $x = \frac{\omega_{pe}^2}{\omega^2} \propto n_e$ and $y = \frac{\omega_c}{\omega} \propto B_0$.

From the solutions, the microwave propagation and damping properties can be explained considering the values of the electron density, magnetic field and the angle of propagation. By the definition, the refractive index (N) has to be positive for enabling the microwave to propagate in plasma. The two different values for the refractive index $N = 0$ and $N = \infty$ imply the cut-off and the resonance conditions for the microwave, respectively. From Eq. (18), three different types of cut-offs can be obtained by putting $N = 0$ that depends on the plasma parameters. Three cut-offs are: (1) $\omega = \omega_{pe}$; this cut-off is also known as 'O' cut-off; (2) $\omega = \omega_R = 0.5\sqrt{\omega_c^2 + 4\omega_{pe}^2} + \omega_c$; this cut-off is also called upper or R cut-off frequency that occurs both above ω_{pe} and ω_c; and (3) $\omega = \omega_L = 0.5\sqrt{\omega_c^2 + 4\omega_{pe}^2} - \omega_c$; it is also called the lower cut-off or L cut-off for the microwave. Based on the local plasma density values and magnetic field values in the plasma volume, "ordinary waves" have 'O' cut-off region, and extra-ordinary waves have two cut-offs, R cut-off, and L cut-off regions, from where corresponding waves are reflected back. To satisfy resonance condition ($N = \infty$), it is found from Eq. (18) that the term $Pcos^2\theta + S sin^2\theta$ has to be zero. It gives the resonance angle in terms of the plasma parameters that are given by:

$$cos^2\theta = \frac{x + y^2 - 1}{xy^2} \tag{19}$$

It is clear that the wave can resonate at the resonance angle (θ) that is decided by the angle of microwave propagation with respect to the magnetic field. From Eq. (18), it is also confirmed that only the extraordinary wave can have the resonances. From Eq. (19), the resonance angles for the extraordinary wave are determined by the plasma density and the magnetic field. For example, if the resonance angle is set to be zero, it is verified that the resonance takes place at $\omega = \omega_{RF} = \omega_c$. This means the microwave matches the larmour frequency of the electrons that are gyrating around the magnetic field lines. It is also known as electron cyclotron resonance (ECR). Again, for the resonance angle, $\theta = 90°$, another type of resonance can occur when $x + y^2 - 1 = 0$, and this condition yields the resonance frequency to be $\omega = \omega_{RF} = \sqrt{\omega_c^2 + \omega_{pe}^2}$. This type of resonance is known as upper hybrid resonance (UHR) applicable to the wave (e.g., extraordinary wave) that is propagating perpendicularly with respect to the magnetic field. The resonance of the ordinary wave can also be understood from Eq. (18). It can be seen from one of the solutions obtained from Eq. (19) that another resonance can exist in the region where $x, y \geq 1$. This is the forbidden region for the ordinary wave, which is the 'O' cut-off region. Therefore, the ordinary-type microwave can reach this resonance only by tunneling through this cut-off region.

To visualize the cut-offs and resonances for the different types of microwaves in a better way, the dispersion plots are shown in a single diagram, also known as Clemmow-Mullaly-Allis (CMA) diagram. **Figure 1** is applicable to the 'cold plasma' approximation case as discussed before. In the CMA diagram, the x- and y-axes represent the plasma density and the magnetic field, respectively. It means that for a given launch microwave frequency, a point on the diagram dictates the experimental situation that is characterized by a particular plasma density and the magnetic field. The diagram is divided into two regions: underdense and overdense plasma regions that are based upon the launch microwave frequency. The boundaries shown in the diagram correspond to the cut-off and resonances for the different types of microwaves.

The polarization of the electric field of the microwaves also plays important role on the damping of microwave power into the plasma. From Eq. (17), the relation between the x- and y-components of the electric field can be found out to understand the polarization in the plane perpendicular to the magnetic field. The relation is obtained from Eq. (17) as:

$$\frac{iE_x}{E_y} = \frac{N^2 - S}{D} \tag{20}$$

Eq. (20) indicates that the waves become circularly polarized and linearly polarized when the cut-off condition ($N^2 = 0$) and the resonance condition ($N^2 = \infty$) are satisfied respectively. The waves are circularly and linearly polarized, respectively. However, it is confirmed that the ordinary waves are left hand polarized and the extraordinary waves are right hand polarized. The electric field of the right hand polarized waves and the electrons gyrating across the magnetic rotate in the same direction. Therefore, if the microwave-launched frequency matches the electron gyration frequency, electrons observe a constant electric field at the resonance location and are resonantly accelerated by the electric field. It is known as electron

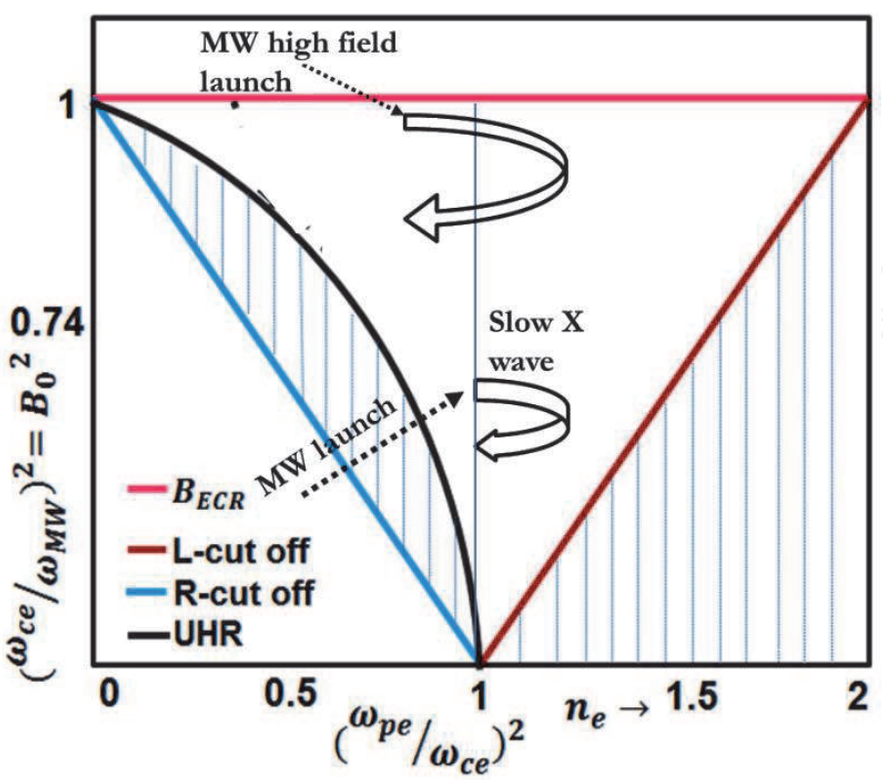

Figure 1.
The CMA diagram shows the propagation of microwave launched from high and low magnetic field side. The arrow bend implies the cut-off region and the mode conversion region near the upper hybrid resonance location.

cyclotron resonance heating (ECR). It is to be noted that only in the ECR heating mechanism the energy is transferred directly from the microwave to the gaseous electrons. As the electrons gain sufficient energy by resonance, they ionize the neutral gases and thus form plasma. There are also other mechanisms for energy transfer from the microwave to the plasma. But the direct energy transfer is not possible in these cases. In fact, the energy is shared among the microwave and the plasma oscillation modes by means of collisional absorption or non-linear phenomenon. The plasma oscillation modes are excited by the '*O*' and '*X*' modes of microwaves. A detailed description of the energy damping mechanisms is discussed below.

2.2 Electron cyclotron resonance (ECR)

As discussed above, the ECR heating is an attractive tool in direct energy transferring to the plasma specifically in the ion source applications. The working principle of ECR mechanism is based on the frequency matching condition in which the microwave frequency with same polarization matches with electron cyclotron motion. It looks pretty much simpler in a qualitative approximation. But in case of quantification, it appears to be a non-deterministic method. It means along with the frequency, the phase difference between the microwave and electron motion also plays important role in energy transferring through ECR mechanism. Under frequency matching condition, if the phase difference between the microwave and the electron motion is in the same phase, then the electrons are accelerated by the microwave electric field. On the other hand, if it is 180° out of phase, the electrons are decelerated. Practically, the temporal phase difference between the microwave and the electron motion is a random phenomenon. So, it becomes necessary to take an average energy gain temporally of the electrons for several microwave periods. It is demonstrated by several groups worldwide that the average temporal energy gain of the electrons has positive value if the averaging calculation is performed irrespective of the phase difference between the microwave and the electron cyclotron motion. It has been proved that the net energy gain is related non-linearly to the microwave electric field ($\propto E^2$). In ECR heating-based plasma, the collisions in plasma can play important role on the confinement of the plasma particles, thermalizing the plasma particles, and also on the ionization rate. The collision properties of plasma are determined by two physical parameters: mean free path ($\lambda_{mean} = \frac{1}{n\sigma}$) and collision frequency ($? = n\overline{\sigma v}$). Here, $\overline{\sigma v}$ is the product between cross-section and the velocity of plasma particles that is determined from the velocity distribution function (Maxwellian type). The particle confinement time is inversely proportional to the collision frequency. A contradiction arises from these two relations. The plasma can have a temperature even in collision-less case and follow the Maxwellian distribution. In collision-less case, the particle does not collide with each other and so there is no thermalization. But in ECR case, the kinetic energy of electrons increases, but there would be low temperature of the plasma. It suggests that there must be other mechanisms that are involved for the solution of this contradiction.

In most of the ECR ion source plasmas, the plasma is collision-less. But in other ion sources operating at microwave discharge, where the temperature of the plasma is comparatively lower and the pressure is also higher, a complete collision-less approximation is not valid. The other heating mechanisms that are involved in the collisional absorption condition must be taken into account. Considering the collisional term in the equation of motion,

$$m_e \frac{\partial \tilde{v}}{\partial t} = e\left(\tilde{E} + \tilde{v} \times \tilde{B}\right) - m_e \omega_c \tilde{v} \tag{21}$$

Here, ω_c denotes the collision frequency. Then the dispersion relation is modified as:

$$N_{O,X}^2 = 1 - \frac{2x(1+iZ-x)}{2(1+iZ)(1-x) - y^2 sin^2\theta \pm \sqrt{y^4 sin^4\theta \pm 4y^2(1+iZ-x)^2 cos^2\theta}} \tag{22}$$

Here, $Z = \frac{\omega_c}{\omega}$. It can be observed that there is collisional term present in the modified dispersion equation of the wave propagation. This collisional term limits the attainable energy during the ECR heating unlike the collision-less case, as discussed before.

2.3 Wave propagation in warm plasma condition

Although the cold plasma approximation is not valid for the wave dispersion in the region very close to the cut-off, the effect of warm plasma condition cannot be ignored. This is because the wavelength in the latter case is not negligible compared to the scale length of the plasma parameters [14]. At the resonance, where the refractive index is infinity, the wavelength becomes equivalent to the electron larmor radius. So, the finite larmor parameter effect is not negligible and has to be considered. The larmor radius can be written as $ŕ = 0.5(k_\perp^2 v_{th}^2)/\omega_c^2$ where $k_\perp$ denotes the perpendicular component of the wave vector with respect to the magnetic field (Z-direction). For the non-relativistic case assuming the Maxwellian distribution function, the distance of frequency from the nth cyclotron harmonic resonance in terms of the Doppler shift unit is written as $\xi_n = (\omega + n\omega_c)/|k_z|v_{th}^2$. Here k_z represents the z-component of the wave vector. The dielectric tensor is expressed as:

$$\overline{\overline{\epsilon_r}} = \overline{\overline{I}} + \frac{\omega_{pe}^2}{\omega^2} \sum_{n=-\infty}^{n=\infty} \begin{bmatrix} \epsilon_{xx} & \epsilon_{xy} & \epsilon_{xz} \\ \epsilon_{yx} & \epsilon_{yy} & \epsilon_{yz} \\ \epsilon_{zx} & \epsilon_{zy} & \epsilon_{zz} \end{bmatrix} \tag{23}$$

where $\epsilon_{xx} = \frac{n^2}{ŕ}\overline{I_n}Z_n\epsilon_{xy} = -\epsilon_{yx} = in\overline{I_n'}Z_n$; $\epsilon_{xz} = \epsilon_{zx} = -n\sqrt{\frac{2}{ŕ}}\overline{I_n}(1+\xi_n Z_n)$; $\epsilon_{yy} = \left(\frac{n^2}{ŕ}\overline{I_n} - 2ŕ\overline{I_n'}\right)Z_n$; $\epsilon_{yz} = \epsilon_{zy} = -i\sqrt{2ŕ}\overline{I_n}(1+\xi_n Z_n)$; $\epsilon_{zz} = 2\xi_n\overline{I_n}(1+\xi_n Z_n)$.

Here $Z_n = Z(\xi_n)$ and $\overline{I_n} = e^{-ź}I_n(ź)$ where I_n is the modified Bessel's function of nth order and Z is a function that is written as [15] $Z\left(\xi_j\right) = \frac{1}{\sqrt{\pi}}\int_{-\infty}^{\infty}\frac{e^{-s^2}}{s-\xi_j}$.

This dielectric tensor coming from warm plasma approximation has few new features that affect the wave propagation unlike the cold plasma approximation case. It can be seen from Eq. (23) that the dielectric tensor is not only a function of ω_{pe} and ω but also a function of the plasma temperature and the k-vector components. So, the dispersion relation yields a new kind of solution that is called electrostatic wave.

2.4 Electrostatic wave

Usually, the electric field of an electrostatic wave does not change with time. This fact is known from the derivation of the electrostatic field from a scalar

potential ($\tilde{E} = -\tilde{\nabla}V$), which makes $\tilde{\nabla} \times \tilde{E}$ to be zero. However, the time-dependent electric field is sometimes denoted as electrostatic wave as it obeys $\tilde{E} = -\tilde{\nabla}V$ relation. So a concrete example for calling an electric field to be electrostatic is the k-vector direction of electrostatic wave with respect to its electric field. If the k-vector is parallel to the electric field, it is called as an electrostatic wave. It means $\tilde{\nabla} \times \tilde{E} = \tilde{k} \times \tilde{E}$ that makes the $\frac{\partial \tilde{B}}{\partial t}$ component to be zero. Therefore, the electrostatic wave does not have any magnetic field component.

A commonly occurred electrostatic wave in a warm plasma condition is named as the Langmuir wave [16]. The Langmuir wave is the main constituent of un-magnetized plasma that appears together with the ion-acoustic wave (IAW). In case of magnetized plasma, electrostatic waves are also present. In this case, if the electrons are displaced by some force, an electric field builds up to restore the electrons back to their initial position to maintain the plasma quasi-neutrality condition. Due to the very low inertia, the electrons will show an overshoot and oscillate around an equilibrium position. The frequency of oscillations is equivalent to the electron plasma frequency of the plasma. The dispersion relation of the Langmuir wave is written as [16]:

$$\omega_L^2 = \omega_{pe}^2 + \frac{3}{2}k^2 v_{th}^2 \tag{24}$$

As the electron plasma oscillates very fast compared to the massive ions present in plasma, the massive ion motion is considered to be fixed in the GHz frequency scale (Langmuir frequency range). Although the frequency of the massive ion motion is very low compared to the Langmuir wave, the massive ions part will take part in the oscillations due to the electric field build-up. This low-frequency oscillations fall usually in the range of ion-acoustic wave frequency. The ion wave dispersion is obtained from the fluid equation as,

$$\frac{\omega_{\mathrm{IAW}}}{k_{\mathrm{ion}}} = \{k_B(T_e + \gamma_i T_i)/M_i\}^{1/2} \tag{25}$$

Usually, the plasma oscillations in the ion-acoustic frequency range lie in between few kHz to tens of MHz.

There exists another kind of electrostatic wave in magnetized plasma, which is known as electron Bernstein waves (EBW). EBW exist in warm plasma conditions when the electron temperature has finite value. It is known that the superposition of the static magnetic field with the oscillating electric field of the plasma waves can make the electron orbit to be elliptical [17, 18]. Now, if the magnetic field is increased further, the electron orbit will become a circular one as the Lorentz force dominates the electrostatic component [17, 18]. The presence of EBW makes the electron gyrophase to organize in such a manner that the space charge distribution in plasma obtains a minima and maxima in the direction perpendicular to the externally applied magnetic field. It was shown [19] that the space charge accumulation is periodic. The charge accumulation propagates with a wavelength that is four times the electron larmor radius [19]. As the wavelength of the EBW is much lower than the length of a typical Langmuir probe tip, used for the plasma characterization, the Langmuir probe is unable to detect the EBW wave directly [20]. The dispersion of electron Bernstein wave (EBW) can be written as:

$$\frac{k_\perp^2}{2\omega_{pe}^2/v_{th}^2} = 2\omega_c^2 \sum_{n=1}^{\infty} n^2 \frac{e^{-b} I_n(b)}{\omega_{MW}^2 - n^2\omega_c^2} \tag{26}$$

Here $k_{\perp}$, v_{th}, and I_n represent k-vector perpendicular component, electron thermal velocity and the Bessel's function, respectively. From Eq. (26), it can be seen that the k-vector becomes infinite at the cyclotron harmonic, i.e., $\omega_{MW}^2 = n^2\omega_c^2$. Therefore, the EBW waves can have resonance at the harmonics of the cyclotron resonance frequencies. In microwave ion source, the resonance absorption of the EBW is possible at the harmonics of the cyclotron frequencies of the ECR magnetic field (B_{ECR}) value.

2.5 Mode conversion theory

In microwave-generated magnetized plasma, the presence of plasma density gradient and the variation of the magnetic field make the wave propagation and its energy absorption unpredictable. It is difficult to estimate the wave trajectory from the simple linear uniform plasma theory [21]. It is natural that the wave would cross the boundaries shown in the CMA diagram by travelling up or down depending on the magnetic field variation and plasma density distribution. Inhomogeneous and anisotropic plasma can exhibit a wide variety of possibilities for the cut-off, resonance, cut-off-resonance and/or the back-to-back cut-off pairs. In inhomogeneous plasma, two or more waves can coexist that propagates in the plasma having density gradient. Although their polarization and propagation vector are different from one another, they can exhibit identical characteristics at some particular plasma regions having particular plasma loading conditions. At those particular scenarios, the waves can remain no longer distinguishable and therefore can convert into another. The mode conversion theory deals with establishing resonance characteristic in inhomogeneous plasma considering two different waves present in the plasma by taking into account the wave reflection, cut-off, resonance and absorption conditions. As the microwaves that are present in the microwave ion source plasma is dominated by the ordinary- and extraordinary-type microwave, the mode conversion theory is mainly focused upon considering the cut-off-resonance pair condition in plasma. The *X* mode microwave is unable to propagate the dense plasma because it is reflected at R cut-off. On the other hand, O-mode microwave is able to propagate in the dense plasma, where it converts into the X mode microwave under certain condition that is obtained from Eq. (18). As per CMA diagram, the *X* mode can have resonance at the UHR region. Therefore, before entering the UHR region, the launched microwave can convert into the *X* mode based on the following mechanisms:

- If the *X* mode microwave is launched from the high magnetic field side, the *X* mode will not see the R cut-off (see **Figure 1**). It will propagate toward the UHR zone where it can convert into an EBW and an ion wave as per the literature. This method is known as *X-B* conversion process.

- Another method in generating the EBW and ion wave is the *O-X-B* mode conversion process. In this process, the *O* mode microwave launched from the vacuum side crosses the R cut-off and converts into a slow *X* mode after tunneling through the evanescent layer. The generated slow *X* mode is then converted into an EBW and an ion wave near the UHR layer.

In microwave ion source plasma under mirror magnetic field configuration, there can coexist two types of components (*O* and *X* modes) of the launched microwave. The ion source cavity acts as a resonator having comparable cavity dimension with respect to the launch microwave wavelength. Therefore, different

types of propagating modes can coexist in the presence of plasma. This makes it difficult to identify which mechanism is actually allowing the X mode to reach the UHR region. However, it is possible to estimate this mode conversion efficiency. For the case of X mode microwave, the refractive index is written as:

$$\frac{c^2k^2}{\omega^2} = 1 - \frac{\omega_{pe}^2}{\omega^2}\frac{\omega^2 - \omega_{pe}^2}{\omega^2 - \omega_{UHR}^2} \tag{27}$$

Let us suppose the X mode wave sees cut-off at the electron plasma frequency, ω_{pe1}. The wave cut-off condition yields

$$\frac{\omega_{pe1}^2}{\omega^2} = 1 - \frac{\omega_c}{\omega} \tag{28}$$

After reflection at the cut-off, the wave propagates in the inhomogeneous and anisotropic plasma in the location where it will find a resonance (refractive index = ∞). The resonance is called upper hybrid resonance where electron plasma frequency is ω_{pe2}. The corresponding Eq. (27) becomes then

$$\frac{\omega_{pe1}^2}{\omega^2} = 1 - \frac{\omega_c^2}{\omega^2} \tag{29}$$

By dividing Eq. (28) by Eq. (29), one gets

$$\frac{\omega_{pe2}^2}{\omega_{pe1}^2} = 1 + \frac{\omega_c}{\omega} = \frac{n_{e2}}{n_{e1}} \approx 1 + \frac{\Delta x}{L} \tag{30}$$

where Δx and L denote the distance between the cut-off and the upper hybrid resonance layer and the length parameter, respectively. From Eq. (30), one obtains

$$\Delta x = \frac{\omega_c}{\omega}L \tag{31}$$

Now, for the wavelength $\lambda \ll L$, the Δx will be many times the wavelength. So the wave will not be able to reach the upper hybrid resonance point. The mode conversion efficiency is determined by the penetration depth of the wave into the plasma. The effective mode conversion can be achieved when the parameter L is comparable to the wavelength, λ. In another way, from Eq. (31), it is also seen that mode conversion can be improved if the magnetic field is reduced.

If a strong electromagnetic field is present in the ion source cavity, the plasma particle follows the relation $v_E \leq v_{the}$; $v_E = eE/m\omega$, where v_E, E, e, m and v_{the} are wave phase velocity, electric field intensity, electron charge, electron mass and electron thermal velocity, respectively. This condition leads to plasma parameters to vary with time. In effect, the non-linear effect such as parametric instability comes into play. Off-course, the parametric decay happens above certain threshold value of the electric field and the microwave energy is shared among the plasma waves and the microwave through the non-linear interaction phenomenon.

2.6 Parametric decay

As the plasma parameters vary with time under the conditions of intense electric field of the microwave, the corresponding velocity becomes close to the electron thermal velocity. It is known that the X mode electric field accumulates near the

UHR region with time due to its propagation from the cut-off region to the UHR region. The accumulated electric field will be able to share some part of its energy through non-linear interactions to the oscillating modes present in the plasma. This non-linear energy coupling between the *X* mode microwave and the oscillation modes is known as parametric instability. It is demonstrated that the *X* mode through this type of instability couples energy to the Bernstein wave and ion wave near the UHR region. The *X* mode normally contains the longitudinal component of the electric field (TM type). Considering the x-component of the *X* mode propagation from Eq. (17), the dispersion of *X* mode wave can be written as follows:

$$(\omega^2 - \omega_{UHR}^2)E_x + i\frac{\omega_{pe}^2\omega_c}{\omega}E_y = 0 \tag{32}$$

From Eq. (11), as the *X* mode approaches the UHR, the term $\omega^2 - \omega_{UHR}^2 \to 0$ and so E_y would be zero. Therefore, the component E_x will remain non-zero at the UHR, which is directed in the direction of propagation of *X* mode. This means the *X* mode at the UHR becomes electrostatic. The *X* mode microwave that becomes an electrostatic wave at the UHR matches with the Bernstein wave and the ion wave. With the two oscillation modes that are coupled with the *X* mode electric field (E_0), the motion of one of the modes (Bernstein wave) can be expressed in terms of the simple harmonic oscillator.

$$\frac{d^2x_1}{dt^2} + \omega_1^2 x_1 = C_1 x_2 E_0 \cos\omega_0 t \tag{33}$$

Here the motion of the first oscillator (amplitude x_1 and the resonant frequency ω_1) is driven by the time-dependent electric field of the *X* mode and the amplitude (x_2) of the second oscillator. The equation of the motion for the second oscillator x_2 is:

$$\frac{d^2x_2}{dt^2} + \omega_2^2 x_2 = C_2 x_1 E_0 \cos\omega_0 t \tag{34}$$

Let us assume, $X_1 = \overline{x_1}\cos\omega' t$ and $X_2 = \overline{x_2}\cos\omega'' t$. In the absence of any non-linear interaction, it can be expressed as $\omega' = \omega_1, \omega'' = \omega_2$ and $\omega_0 = \omega_1$. But in the presence of non-linear interaction, this is incorrect. For the case of non-linear interaction, as the driving terms cause frequency shifting, the frequency ω_2 is approximately equal to ω''. However, in the absence of non-linear interaction, the solution from the system of coupled Eqs. (33) and (34) is obtained as:

$$\omega'' = \omega_0 \pm \omega' \tag{35}$$

Now if ω' is small such that both values of ω'' lie within the bandwidth of oscillator, x_2, there exist two oscillators: $x_2(\omega_0 + \omega')$ and $x_2(\omega_0 - \omega')$. Under this assumption, solving the coupled Eqs. (33) and (34), the following frequency matching condition is arrived:

$$\omega_0 \cong \omega_2 \pm \omega_1 \tag{36}$$

As the oscillators are waves, the '?t' term is replaced by '(?t-$\tilde{k}.\tilde{r}$). Following this, a new matching condition of k-vector is reached, $\tilde{k_0} = \tilde{k_2} \pm \tilde{k_1}$.

The frequency and k-vector matching conditions correspond to the energy conservation and momentum conservation following the quantum mechanics theory. It is proved that [15] the *X* mode generates two waves through parametric decay: a

high-frequency Bernstein wave and a low-frequency ion wave following the frequency matching condition. This leads to the generation of secondary peaks around the launched microwave frequency, which is called as sideband. Therefore, the simultaneous presence of the sideband peaks around the launched frequency signifies the parametric decay near the mode conversion region.

The parametric decay occurs above a certain threshold value, which actually depends on the damping rate of the oscillator. If the damping rates Γ_1 and Γ_2 for two oscillators x_1 and x_2, respectively, are introduced in Eqs. (33) and (34), one can conclude that the lowest threshold occurs at the exact frequency matching condition. The corresponding threshold electric field is obtained as [19]:

$$C_1 C_2 E_{0threshold}^2 = 4\omega_1\omega_2\Gamma_1\Gamma_2 \tag{37}$$

2.7 Damping of electrostatic and electromagnetic energy

Electrostatic waves generated in the plasma through the parametric decay instability can damp their energy to the plasma particles and thus increase the plasma density. When the phase velocity of the electrostatic wave becomes comparable to the thermal velocity of the plasma particles, the energy is transferred from the wave to the plasma particles and is known as Landau damping mechanism. In microwave ion source plasma, density can be increased 2–3 times more than the ECR heating mechanisms through the off-resonance heating mechanism. For this reason, the off-resonance condition is used to create favorable conditions of the upper hybrid resonance heating. Under certain plasma temperature, the electrostatic wave can transfer energy resonantly to the plasma particles if the wave phase velocity matches the plasma particle velocity. In some cases, the plasma particle velocity can be higher than the wave phase velocity. Under this condition, the plasma particle can transfer energy to the wave. The Landau damping mechanism follows the equation written below:

$$I_m\left(\frac{\omega}{\omega_{pe}}\right) = -0.2\sqrt{\pi}\left(\frac{\omega_{pe}}{kv_{th}}\right)^3 e^{-12k^2\lambda_D^2} \tag{38}$$

The exponential term on the right hand side represents that the Landau damping will be small for small value of $k\lambda_D$. The Landau damping phenomenon is applicable for both case of electrons and ions. The electrostatic wave whose frequency falls in the range of electrons can heat the electrons only in the parallel direction with respect to the magnetic field. In case of electrostatic ion wave, such restriction does not apply. This is because the electrons are strongly magnetized and so will not be able to move across the magnetic field.

In case of a compact microwave plasma device where the microwave wavelength becomes comparable to the device dimension, the cavity resonant mode can also play crucial role in damping the electromagnetic energy to the plasma particles. The presence of multiple cavity modes in the plasma can produce modulated wave due to the interaction between each pairs of the cavity resonant modes. The generated modulated wave propagates in the plasma and damps its energy to the plasma particles where the frequency of the modulated wave matches the local plasma frequency of the plasma particles.

3. Simulation modeling of MW interaction in plasma

For the MW interaction modeling during the plasma evolution, a schematic of the computational domain is shown in **Figure 2**. The computational domain consists

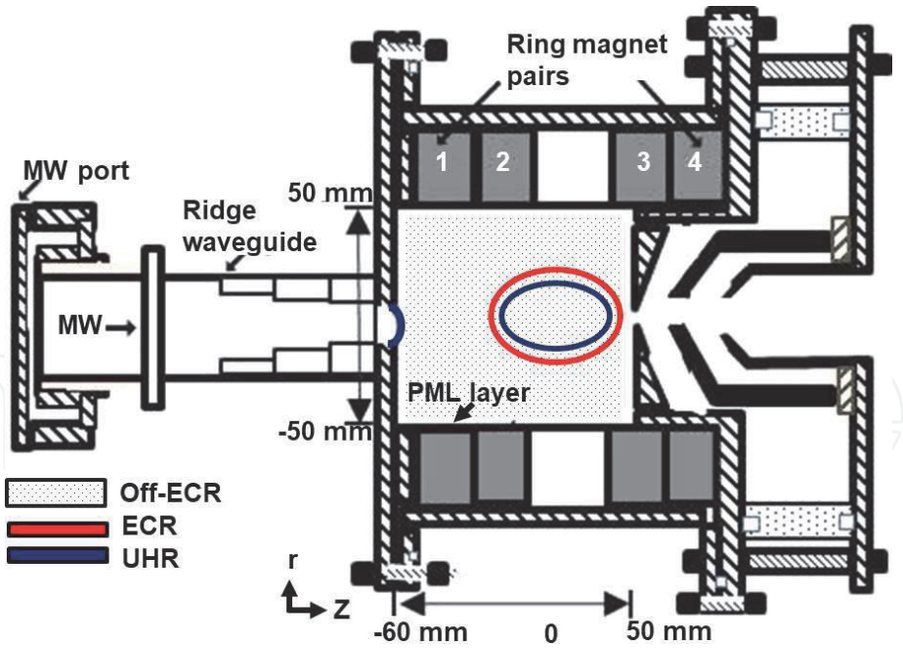

Figure 2.
Simulation domain of the MW ion source.

of a microwave coupled reactor, which is a cylindrical plasma cavity. A MW of frequency 2.45 GHz is injected into the microwave coupled reactor through a ridge waveguide port (on the left side of **Figure 2**) to ionize the gaseous particles, thus forming the plasma that is confined under the mirror magnetic field configuration. The reactor has dimension of 107-mm and 88-mm diameter. The microwave power is fed into a cavity resonator through a tapered waveguide. The waveguide is tapered by embedding four ridge sections having different ridge length, ridge gap and ridge width on the inner sidewalls of the waveguide. The ridge dimensions are optimized from the analytical calculation as well as from the electromagnetic simulation. The mirror magnetic field is created by using two pairs of ring magnets that surround the microwave coupled reactor [22]. On the right side of the microwave coupled reactor (**Figure 2**), the ion beam extraction system is attached through a 5-mm hole on the wall of the reactor. The similar computational domain is used in the experimental set-up (Section 5) to validate the simulated data. Here, the finite element method (FEM)-based COMSOL model is used [22].

The MW propagation and the plasma evolution are assumed to be decoupled to each other during the simulation modeling in the temporal scale [10]. The MW electric fields ($\vec{E}$) are averaged for some MW periods before putting their value in the plasma model and the resultant field is given as input to the plasma model. The electron's momentum equation is time integrated along with Maxwell's equations for some MW periods until the MW model of the FEM gets a periodic solution of the equation to transfer an average power to the particles over such a period. The FEM model continues this process until it gets a steady state solution for at least $\sim 10^3$ ($\omega/\nu_m \sim 10^3$) MW periods. Here, ω is MW frequency and ν_m is electron's momentum transfer frequency. Since the electrons stay in the ECR zone for a very short time (transit time) duration, it causes non-local kinetic effects. This results in the de-phasing between the velocity and field oscillations that becomes very difficult to describe using the fluid model. This problem is resolved by introducing the effective collision frequency (ν_{eff}) in the simulation to converge the solution. In the low pressure condition, for the collision-less heating, ν_{eff} has to be in the order of inverse transit time for the electrons [10].

In case of MW model, the equations for the electric field are solved in frequency domain while keeping the other parameters in time domain. In the beginning, the FEM model started from the Maxwell's equations in order to justify the modeling approach. The MW electric fields are changing with time at a frequency of $\omega/2\pi$. During the plasma evolution, the total electric field (E) value in the μs time zone is regarded as a resultant quantity (or total) that comes from the superposition between the MW and ambipolar-type electric field of the plasma. The modification of the resultant electric field follows the equation that is given below:

$$\nabla \times \mu^{-1} (\nabla \times E) - k_0^2 \left(\varepsilon_r - \frac{i\sigma}{\omega \varepsilon_0} \right) E = 0 \tag{39}$$

The notations used in the above equations $k_0, \varepsilon_r, \sigma$ *and* E are the vacuum wavenumber, relative permittivity, the total electric field and the plasma conductivity in full tensor form, respectively. This plasma conductivity is a function of plasma density, collision frequency and B-field. So, all types of total electric field components are possible to estimate as the FEM model can determine the above parameters for some particular plasma loading conditions during its evolution. The model also considers that the $\tilde{E}$-field evolution in the sub-nanosecond region is well separated from the total E-field quantity. This means the total E-field changing during the μs region is composed of the MW electric field and the ambipolar electric field.

For representing the MW propagation in an infinite space, the perfectly matched layers (PML) are introduced in the computational domain as shown in **Figure 1**. The present FEM model considers the electron transport properties to follow the Boltzmann distribution function. The distribution is an integro-differential equation in phase space (r, u) that cannot be solved efficiently. For this reason, the FEM model assumes the plasma as a fluid following the drift diffusion approximation. The assumption is adapted from the Boltzmann equation that is multiplied by some weighing function and then integrated the resulted function over the velocity space. This exercise yields completely three-dimensional and time dependent equations [10, 23]. During the modeling, FEM assumes that ion motion is negligible with respect to the electron motion in the timescale (ns) of MW. Additionally, the electron density is constant spatially within the ECR surface. The Debye length is also assumed to be much smaller than the interaction length of the MW. The average value of the electron velocity on the microwave timescale is obtained from the assumption of Maxwellian distribution function and from the first derivative of the Boltzmann equation. The following drift-diffusion equations are shown that are used to compute the electron density and electron energy density:t

$$\frac{\partial n_e}{\partial t} + \nabla.[-n_e(\mu_e.E) - D_e.\nabla n_e] = R_e \tag{40}$$

$$\frac{\partial n_\varepsilon}{\partial t} + \nabla.[-n_\varepsilon(\mu_\varepsilon.E) - D_\varepsilon.\nabla n_\varepsilon] + E.\Gamma_e = R_\varepsilon \tag{41}$$

The term in Eq. (42) is $E.\Gamma_e = en_e v_e \cdot E_{ambipolar} - \Pi$. This is a heating term $E.\Gamma_e$ that comprises two components. The first component means the electrons are getting energy through the ambipolar field during the plasma evolution. The second component (Π) signifies the MW absorption power $(n_e \langle v_e \cdot \tilde{E} \rangle)$ that is carried by the electrons in the plasma. The other terms $n_e, v_e, R_e, \Gamma_e, \mu_e, \mu_\varepsilon, E, D_e, n_\varepsilon, R_\varepsilon, \Gamma_\varepsilon, n_\varepsilon$ and D_ε are the electron density, average electron velocity, the source term of the electrons, electron flux, the mobility of the electrons $(4 \times 10^4\ m^2/(Vs))$, electron

energy mobility, total electric field, electron diffusivity, electron energy density, energy loss/gain from inelastic collisions, electron energy flux, electron energy mobility and electron energy diffusivity, respectively. Some of the terms described above, the electron's diffusivity, mobility and energy diffusivity, are estimated following the relations that are given below:

$$D_e = \mu_e T_e; \mu_\varepsilon = (5/3)\mu_e \text{ and } D_\varepsilon = \mu_\varepsilon T_e \tag{42}$$

The above written electron transport properties represent full tensor parameters in which the tensor term electron mobility is influenced by the magnetic field. The electron mobility without the magnetic field $\left(\equiv 1 \times 10^{25}/N_n\right)$ and with the magnetic field is the known parameters. Here, N_n represents the neutral density of the gaseous particles. The electron source term in Eq. (40) is obtained from the relevant plasma chemistry that is expressed below with the help of the rate coefficients $R_e = \sum_{j=1}^{M} x_j k_j N_n n_e$. The presented symbols M, x_j and k_j represent the number of reactions, the mole fraction of a specific species and the rate co-efficient for the reaction j, respectively [10]. The energy loss terms as shown in Eq. (41) is written for all the reactions as $R_\varepsilon = \sum_{j=1}^{M} x_j k_j N_n n_e \Delta\varepsilon_j$. The notation $\Delta\varepsilon_j$ denotes the energy loss that occurs from the reaction j. The energy source and the loss terms are calculated inherently in the FEM model. The rate coefficients mentioned in the above expressions are taken from the cross-section data as per the relation $k_k = \gamma \int_0^\infty \varepsilon \sigma_k(\varepsilon) f(\varepsilon) d\varepsilon$, where γ is $(2q/m_e)^{1/2}$. In this expression, the symbols m_e, ε, σ_k and f are represented as the mass of electron, energy of electron, cross-section for the reaction and the electron energy distribution function (Maxwellian) for the electrons, respectively.

The description for the boundary conditions taken during the plasma simulation is as follows. The plasma chamber wall is kept at ground potential. The reflections, secondary emission and also the thermal emission from the electrons are assumed to be negligible at the wall boundaries. In effect of that the electron flux and electron energy flux at wall boundary can be written as $n.\Gamma_e = (\frac{1}{2} v_{e,th} n_e)$ and $n.\Gamma_\varepsilon = (\frac{5}{6} v_{e,th} n_e)$, respectively. In addition, the heavy plasma particle losses at the boundary walls and their migration are considered to be originating from only the surface reactions and ambipolar electric field, respectively. A fixed power is maintained that is absorbed by the plasma ($P_{absorbed}$). This is done by re-adjusting the normalization factor (α) during the moment of the plasma evolution (ns to μs). The normalization of the plasma absorbed power follows the relation $P_{absorbed} = \alpha \iiint n_e P_{set}\, dV$. Here, $P_{set} \equiv -e\left\langle \tilde{v}_e . \tilde{E} \right\rangle_t$ is represented as the average set power applied to the cylindrical plasma cavity. This normalization helps in convergence of the solution and avoids any disproportionate absorption of the power by the plasma. Here, a fixed plasma absorbed power of 70 W is chosen to benchmark its results with the experimental findings that are reported taking the boundary conditions [23, 24] similar to the computation system and the operating conditions.

In the MW-plasma simulation model, the instant of MW launch is taken as reference (t = 0 s) when the MW is launched into the cavity. The MW is launched in right (R) hand mode (R mode is extraordinary type) using the four step ridge waveguide. This makes the $\tilde{E}$-field intensity to be maximum in the center of the cavity that is propagating in parallel to the externally applied magnetic field [25, 26]. As soon as the MW is launched, it continues to interact with the gas particles on their propagation timescales (ns). To understand and visualize the profile modification of the electrical field from the start of MW launch to the steady state plasma generation and also their impact on the power coupling to the plasma

with time, total breakdown time is split into some discrete values such as 10 ns, ~67 ns, ~158 ns, 452 ns, 630 ns, ~2 μs, 2.5 μs, 3 μs, ~5 μs, ~8 μs, ~20 μs, ~40 μs, 250 μs and 300 μs. The simulation is exercised with an argon gas. The initial conditions for the calculation of the plasma parameter evolution are plasma density (1×10^{12} m^{-3}) and plasma temperature (~4 eV). These parameters are used initially to estimate the plasma conductivity σ. Then the electric field is estimated by putting the above initial conditions in Eq. (39). The estimated field values are later utilized to find out the temporal variation of different plasma parameters and so electric field components' self-consistency.

The present FEM model uses different solvers sequentially to compute the magnetic field distribution first throughout the computational domain. Then the solvers related to the frequency-transient analysis are used to calculate the MW-plasma parameters. A complete computational flowchart for the magnetic field as well as the MW-plasma is depicted in **Figure 3**. The typical number of degrees of freedom that is used for solving the magnetic field is approximately 54,525. The FEM magnetostatic model uses the equation-based mesh adaptation technique to generate the extremely fine mesh size on the ECR surfaces. The mesh element has

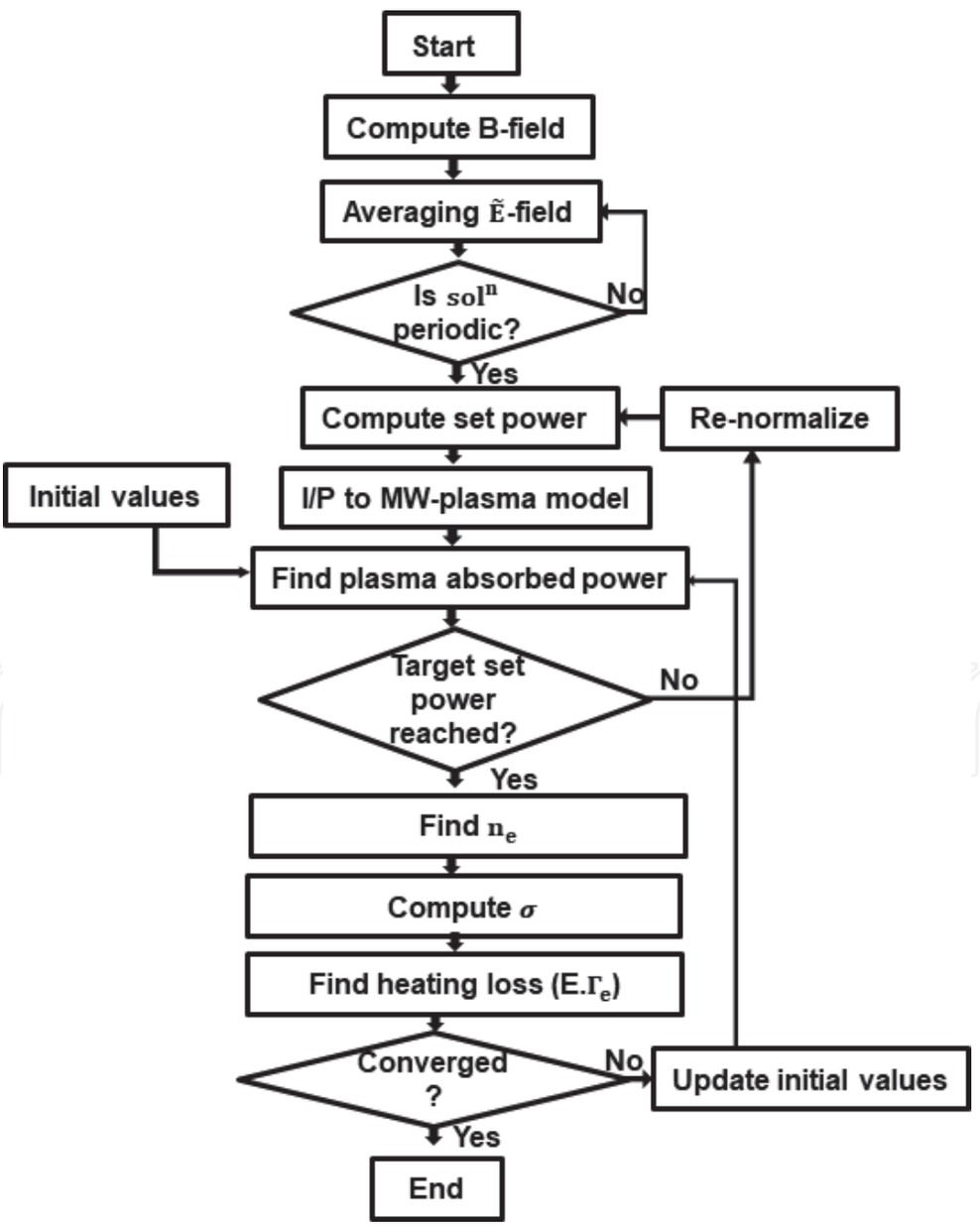

Figure 3.
Simulation flowchart of MW plasma interaction in COMSOL Multiphysics.

minimum and maximum size for the magnetic field and microwave-plasma calculations are 0.2 mm and 2.4 mm, respectively. The effect of the different edges that are involved in the computational domain is taken into account by keeping the maximum and minimum mesh element size at 0.5 mm and 0.0055 mm, respectively. The magnetic field estimated is used in the MW-plasma model to estimate the tensor plasma parameters. For the case of MW-plasma simulation, the number of degrees of freedom used for the solution is approximately 47,005.

Due to the dephasing as discussed above, the current FEM model uses the concept of effective collision frequency (ν_{eff}) to describe the sudden phase decoherence. In the dephasing situation, the phase relationship between velocity and the electric field oscillation is destroyed in the temporal scale due to which the electrons experience a large field variation in the ECR surface. The accelerating electric field transfers energy to the electrons that are residing on the ECR surface only for a small time duration in the time range of resonant cyclotron motion of the electrons. The electrons also experience spatial density variations while oscillating across the ECR surface. A large density variation across the ECR surface also generates the radial ambipolar electric field on the resonance surface and so there is a possibility of de-phasing that can happen at the resonance zone.

As the phase de-coherence may happen between electron gyro motion and the MW oscillatory $\tilde{E}$-field, the electrons get accelerated and deccelerated assymetrically. This temporal asymmetry of acceleration and decceleration in opposite cycle are responsible for transferring an effective energy to the electrons. The effective collision frequency ν_{eff} is estimated using the relation $\nu_{eff} = \sqrt{v_e \omega / \delta_B}$, where v_e is the electron thermal speed and δ_B is the gradient of magnetic field. The value of ν_{eff} is few orders more than that of actual collisional frequency that an electron encounters with the gaseous particles. However, it is to be noted that the effect of ν_{eff} is insignificant on the power absorption profile. Instead it helps in overcoming the numerical instability. For obtaining a steady-state solution, the number of MW periods has to be in the order of ω/ν_{eff}. This makes computation less rigorous than the case of actual collisions, if considered.

The evolution of the radial (E_r) and axial (E_z) components of the electric fields during the plasma evolution plays an important role in the MW coupling to the plasma and so the plasma parameters as discussed above. To support these facts, the

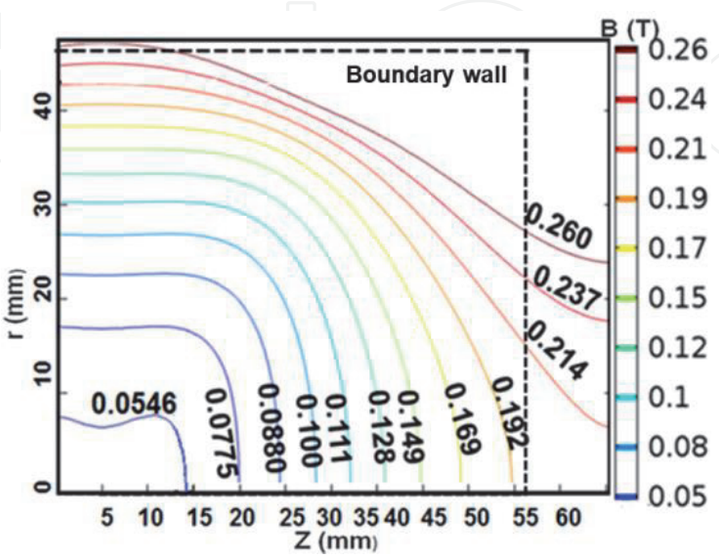

Figure 4.
Magnetic (B) field contour inside the quadrant section of the plasma chamber, which has cylindrical axis symmetry. The B-field is also simulated using COMSOL software. The narrow contour area near 0.088 T line is the ECR zone (corresponding to 0.0875 T). The span of ECR zone is around z = ±24 mm and r = ±28 mm.

evolution of the different components of the electric fields and correspondingly the plasma parameters is shown in the results and discussion section given below to study their effects on the plasma parameters. To understand the resonance zone in the plasma chamber, the required magnetic field contours are shown in **Figure 4**.

4. Results and discussion

This section of the chapter shows the temporal behavior of the electric fields, power deposition and the corresponding variation of plasma density and hot electron temperature from the start of MW launch to the steady state condition.

4.1 Behaviors of total electric field ($|E|$) during plasma evolution

Figure 5(a) and **(b)** shows the evolution of the radial profiles of the total electric field taken on the different axial locations for two time instances, 3 μs and 20 μs, after the MW launch. The radial profiles show the total electric field intensity to be more near the MW launching port (z = −40 mm). As one moves toward the extraction (z = −60 mm), its values is decreased because of the plasma shielding effect.

A sharp change in the E-field is shown in **Figure 5(a)** at the time, t = ~3 μs near the 2.45 GHz ECR surface (r ≈ 23 mm) for the planes, z = ±20 mm. The strong inhomogeneity in the E-field implies the absorption of the MW power at the same locations [27]. The power absorption location is also dependent on the magnetic field profile as well within the cylindrical cavity. Another figure, **Figure 5(b)** shows the radial E-field pattern across the different planes for time, t = 20 μs. The inhomogeneous part of the E-field profile looks similar to **Figure 5(a)** for the case of z = −20 mm plane. But the intensity of the E-field is being reduced with time due to the plasma shielding. One can observe that the inhomogeneous part of the E-field is shifted toward the off-ECR regime (r ≈ 28 mm) from the ECR surface with the increase of time. Therefore, the power absorption region is being shifted from the ECR zone to the off-ECR zone. This effect is visible in the power deposition location throughout the cylindrical cavity in **Figure 6**. **Figure 5(a–d)** shows the corresponding shifting of the power deposition location from the ECR zone to the off-ECR zone or UHR zone with time. As the plasma reaches steady state during the time, t = 20 μs, the evolution of the plasma density and temperature is shown in **Figure 7**.

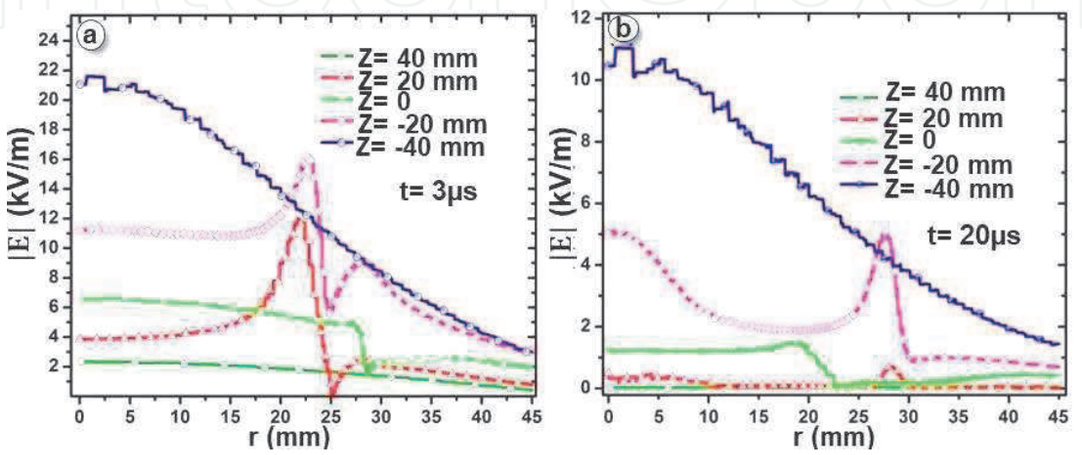

Figure 5.
(a) Total electric field (|E|) magnitude during gas ignition time of ~3 μs, (b) total electric field (|E|) magnitude during gas ignition time of ~20 μs.

4.2 Time evolution of plasma with power deposition

Figure 6a shows that the MW power is being deposited exactly on the ECR (∼0.0875 T) surface corresponding to the launch MW frequency of 2.45 GHz when the plasma density is low. But as time passes (see **Figure 6b–d**), the power deposition location gets shifted in the off-ECR or upper hybrid resonance (UHR) regime. The UHR zone is a region where the two conditions $n_e < n_{crit}$ and $B < B_{ECR}$ are satisfied [26–28]. The term n_{crit} represents the critical density for the MW frequency, 2.45 GHz that is 7.4×10^{16} m^{-3}. If one can compare **Figures 6(c)** and **7(a)**, one can visualize that the plasma density ($\sim 1.3 \times 10^{17}$ m^{-3}) crosses the critical density from ∼2.5 μs onwards and the plasma density that is above the critical density is denoted as overdense plasma. So as the overdense plasma is achieved, the electrons get accelerated by less amount of MW energy on the ECR surface. Correspondingly, the plasma bulk temperature increases from the start of MW launch (t = 0 s) to the instant of ∼630 ns. It is evident from **Figure 7a** that the plasma bulk electron temperature increases and becomes steady near a value of ∼80 eV. Then the plasma bulk temperature decreases in a faster way with further increase of time. Hence, one can conclude that heating through ECR process is being ceased to occur with the further increase in time. The causes to increase the absorbed power density is expected to be highest ($\sim 5 \times 10^7$ W/m^3) on the ECR surface during the time, t = 630 ns.

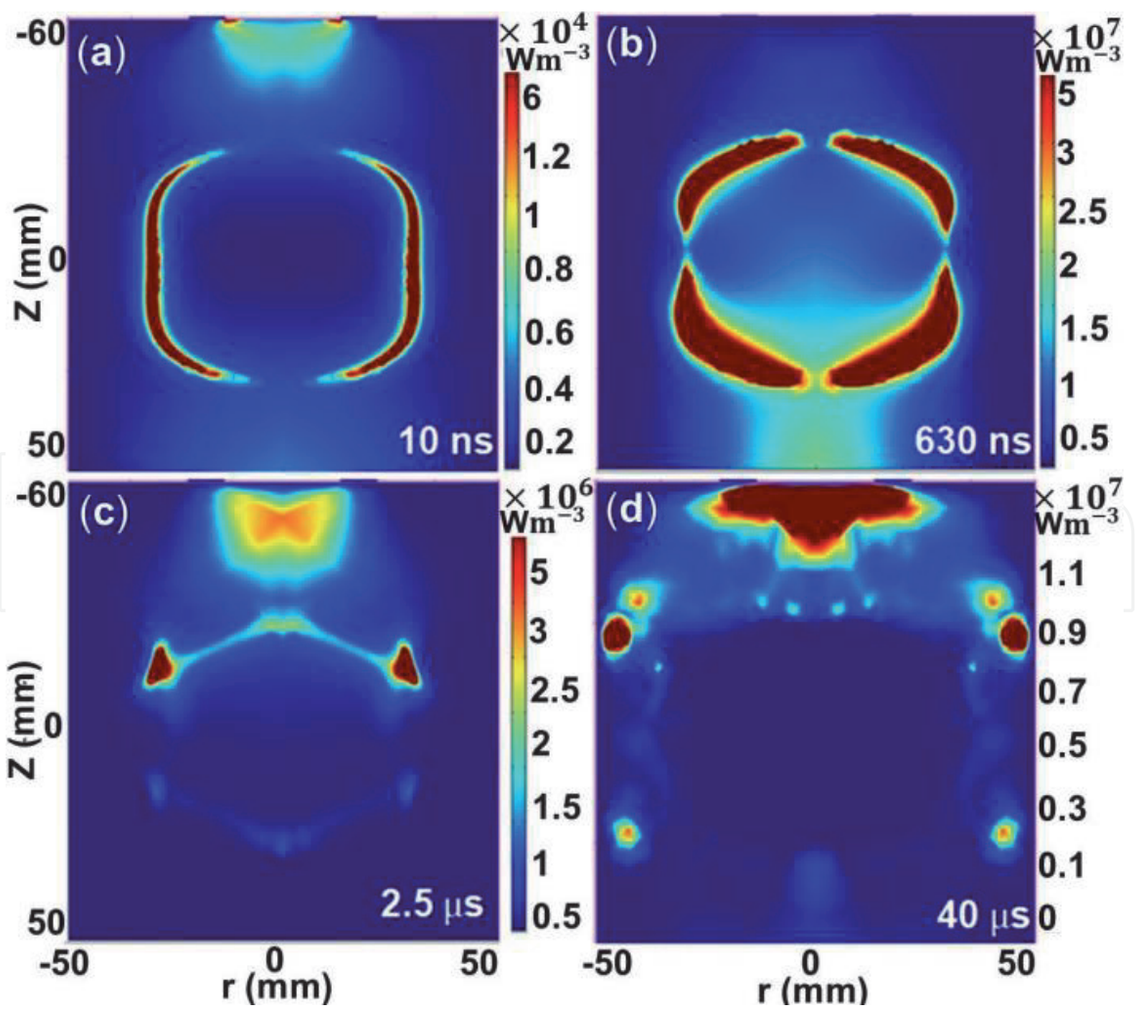

Figure 6.
Power deposition density at different time steps for 70 W of absorbed power. (a) t = 10 ns, peak power density is 6.6×10^4 W/m^3, (b) t = 630 ns, peak power density is 1.43×10^7 W/m^3, (c) t = 2.5 μs, peak power density is 5.12×10^6 W/m^3 and (d) t = ∼40 μs, peak power density is 1.67×10^7 W/m^3.

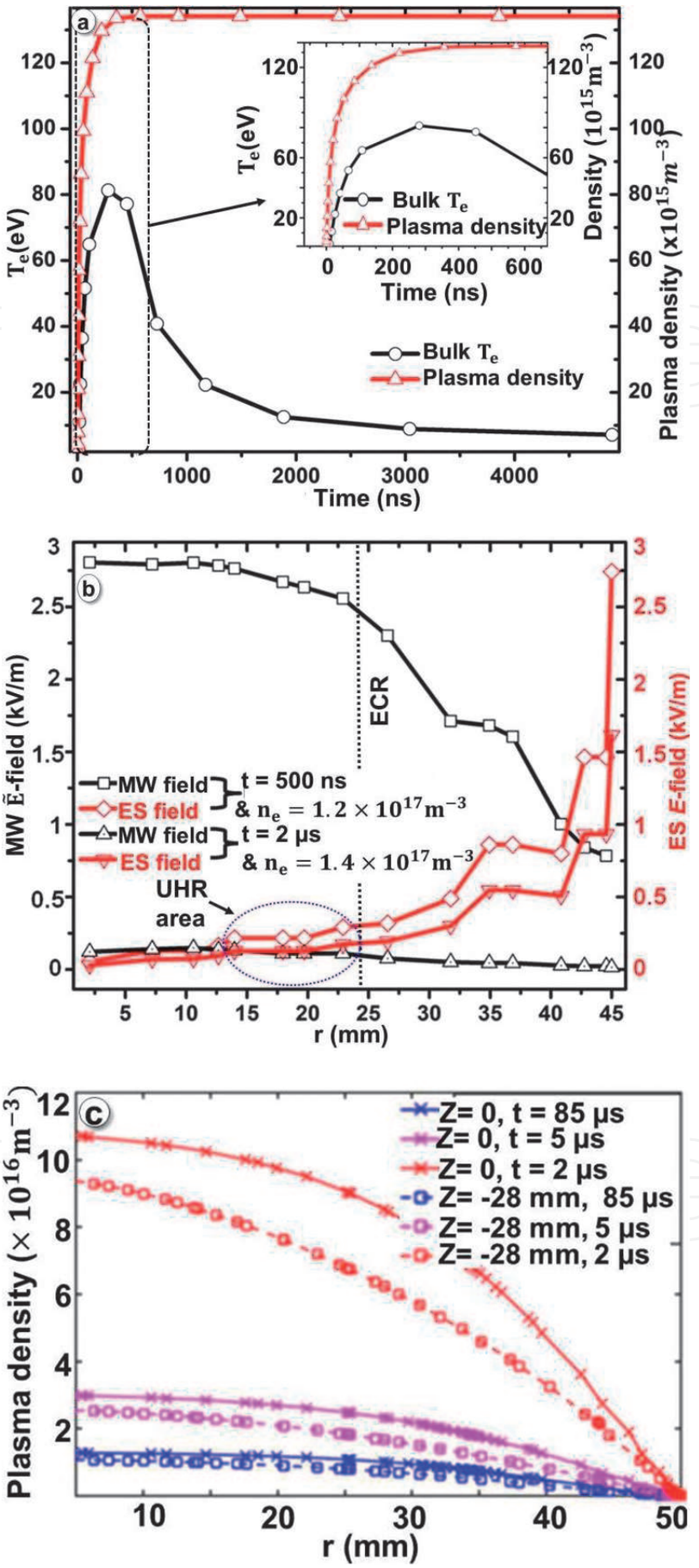

Figure 7.
(a) Temporal evolution of electron density and temperature during plasma formation time at point (r = 0, z = −28 mm) with gas pressure, 2 × 10^{-3} mbar. (b) Temporal variation of MW electric field and plasma generated ambipolar electric field, the two main constituents of total electric field. (c) Radial profile of plasma density at three different time instants (t = ∼2 μs, ∼5 μs and 85 μs), at two axial locations during evolution of the plasma.

Correspondingly, the plasma density also reaches above the critical density. The decrease in the plasma bulk temperature and the corresponding increase of the plasma density even above the critical density are attributed to be occurring from the off-ECR or ES surface wave heating mechanisms [29, 30]. In other words, although the plasma density is approaching steady state (**Figure 7a**), the temperature is not yet stabilized during that time.

To confirm the off-resonance or electrostatic heating methods as discussed above, the evolution of the MW electric field and the electrostatic electric field is shown simultaneously in **Figure 7(b)**. The radial distribution of the two types of the electric field is given in that figure for two discrete time instants and the corresponding plasma densities. One can observe that the MW electric field is significant throughout the cavity and is more than the electrostatic electric field for the time, t = 500 ns. For another instance, t = 2 μs, the electrostatic electric field becomes more than the MW electric field throughout the cavity. The electrostatic field is even more in the upper hybrid resonance locations than the MW field as shown in **Figure 7(b)**. This evidence confirms that the electrostatic heating is being taking place at the UHR region where the magnetic field and plasma density satisfy the above-mentioned conditions [28]. To visualize the plasma density pattern due to these electric field behaviors, the radial distribution of the density is shown in **Figure 7(c)** for different time instances (i.e., 2, 5 and 85 μs) and axial planes on the cylindrical cavity during the plasma evolution. The plane z = −28 mm on the cavity is situated near the MW launching port. **Figure 7(c)** shows the plasma density to be more at the central location (z = 0 mm) than the location z = −28 mm that is located toward the MW launch side.

From the above-mentioned results (**Figures 6** and 7), it can be commented that the power is absorbed by the ECR mechanism especially in the plasma condition where the density is below (underdense plasma) the critical density and slightly above the critical density (overdense plasma). If one notices the plasma parameters for the underdense conditions, one can observe that the density remains below the critical density from the time, t = t = 45 ns to t = 110 ns. In this case, the plasma electrons are magnetized and hence are following the magnetic field lines. The field free zones that are located near (r, z) = (0, 0) are being filled by the plasma particles because of the diffusion processes. Due to the ECR heating, the electron temperature is being increased in the field free zones in the underdense plasma situation, t < 110 ns. As the magnetic field lines are stronger (B ∼ 2300–2600 G) near the radial locations of the cavity, i.e., in the gaps of the two pairs of ring magnets, the plasma bulk electron temperature exhibits a sharp gradient in those regions. The maximum plasma bulk electron temperature achievable is ∼85 eV that occurs during the time, t = 280 ns. The high energy part of the plasma bulk electrons is being concentrated completely in the same gap as mentioned before during this time.

It is observed that the plasma bulk electron temperature increases in the radial direction at the regions mainly in between the two pairs of the ring magnets with the increase in time from t = 280 ns to 730 ns [22]. Therefore, it can be summarized that with the increase in plasma density (or time, t = ∼45 ns to t = ∼280 ns) from underdense to overdense state, the plasma bulk temperature is increased by an amount of ∼80 eV mainly in the radial direction near the region, 24 mm < r < 40 mm, −25 mm < z < 25 mm. This is because the ECR surfaces lie in those regions. The continuous heating through ECR in this location causes the high energy part of the plasma electron temperature to be concentrated on the same location even in the overdense plasma state during the time t = 730 ns.

The anisotropic behavior of the plasma bulk electron temperature even in the overdense plasma signifies the ECR heating [31, 32]. With further increase of time after the MW launch, i.e., near t = 2000 ns, the plasma bulk temperature (T_e) is

decreased to ~10–12 eV. This range lies close to the thermal electron temperature. Therefore, the reduction of the high energy component of the plasma bulk temperature can be argued as the minimal occurrence of ECR heating process and correspondingly the initiation of the electrostatic heating mechanisms in the same time frame [29–31, 33]. The plasma reaches steady state after 2000 ns (2 μs) (**Figure 7a**). At the saturation, the plasma density is approximately 2 times more ($\sim 1.3 \times 10^{17}$ m^{-3}) than the critical density. During the same instant of time, the plasma electron temperature and its gradient reduce in the location where the magnetic field is relatively lower.

In order to investigate the different coupling mechanisms involved during the plasma evolution process and their impacts on the plasma parameters, the behavioral pattern of the different components of the electric field (E_r and E_z) is shown in **Figures 8–10**. The power coupling mechanisms are ECR, UHR and polarity reversal related to ES heating. The particular type of coupling mechanism is understood from the electric field evolution pattern throughout the cavity. The electric field characters can be useful to characterize the plasma parameters based on the theoretical and experimental proofs. The proofs say the higher the plasma density, the more the power absorbed by the plasma.

4.3 E_r-field evolution with time

In **Figure 8(a–c)**, the radial electric field (E_r) variations are shown for three different z-planes of the cylindrical cavity. The figures also show the evolution of the E_r-field profile at different time instances after the MW launching. **Figure 8(a)** gives the E_r profile close to the ECR surface (z = −28 mm), which is also near to the MW launch point (z = −60 mm). Another figure (**Figure 8**(b)) shows the E_r-field profile along the central plane (z = 0) of the cavity, whereas **Figure 8(c)** gives the E_r-field evolution along the plane z = 28 mm that is close to the ion beam extraction point.

In all the figures, a strong inhomogeneity in the E_r-field profile signifies the power absorption locations. Taking a time instant t = 67 ns in all the figures, the presence of the E_r-field throughout the cavity can be visualized since the plasma density at this time has not reached above the critical density. As the plasma density crosses the critical density with advancement of time (>500 ns), the E_r-field profile is being modified following the density evolution pattern. The inhomogeneity in the E_r-field profile is more pronounced in **Figure 8**(b) than in the case of other figures. The difference in the radial variation of the E_r-field comes from the variation of resonance magnetic field contour as shown in **Figure 3**. The strong inhomogeneous part of E_r-field initially very near the ECR surface indicates that the electrons are accelerated by the ECR phenomenon. Then after >2 μs, this inhomogeneous part gets shifted toward the UHR $\left(f_{UHR} = \sqrt{\left(f_{pe}^{\ 2} + f_{ce}^{\ 2}\right)}\right)$ regions where the MW frequency matches the f^{UHR}. The E_r-field value after ~2 μs at r = 0 mm and z = −28 mm location is negligible and so the plasma density reached overdense state, whereas for some regions (UHR regions), as shown in **Figure 8(a)**, the E_r-field component is showing significant intensity. The high value of E_r-field, near the location ($B < B_{ECR}$), represents that the plasma is still underdense in this region during time t = ~3 μs.

Therefore, the dual conditions ($B < B_{ECR}$ and $n_e < n_{crit}$) are satisfied for the UHR heating process. This phenomenon is also being reflected in **Figure 7(a)** and **(b)** as discussed earlier. **Figure 7(b)** shows the electrostatic electric field to grow with the plasma density and correspondingly the MW electric field decreases after

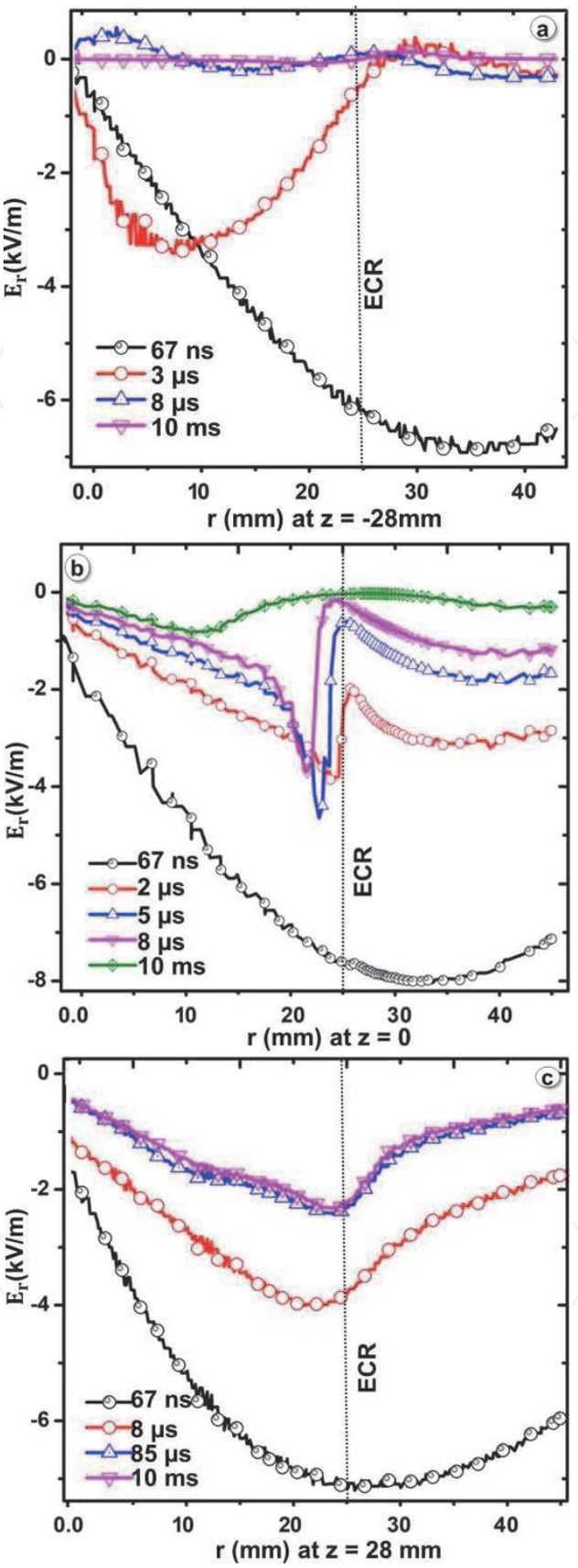

Figure 8.
E_r*-field evolution and its pattern during plasma generation (a) r = −28 mm, (b) r = 0 mm and (c) r = 28 mm.*

500 ns. The electrostatic electric field, the component of the total electric field, is getting increased due to the increase of the plasma ambipolar potential. So this gives a clear evidence of power transferring from MW coupling to the electrostatic wave coupling to the plasma. Since the electrostatic wave does not face any density

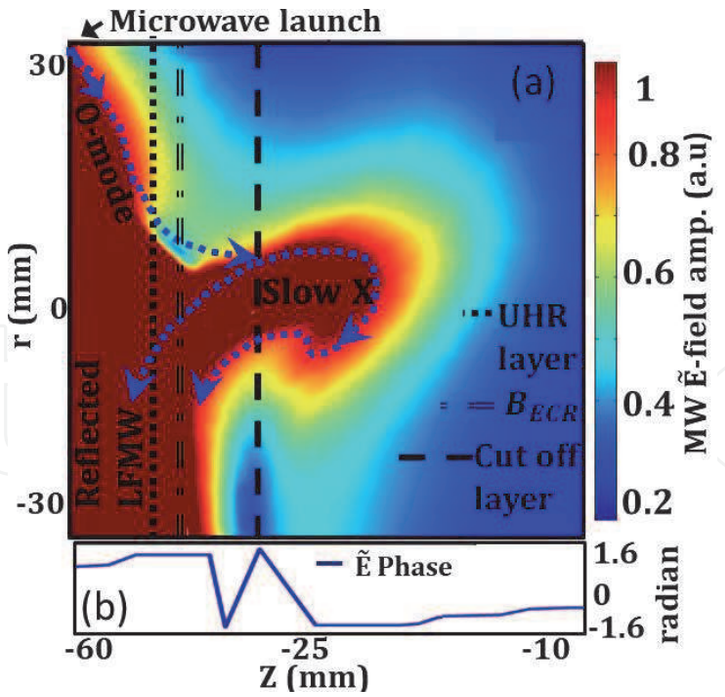

Figure 9.
(a) Propagation and mode conversion of MW Ẽ-field corresponding to an ordinary (O)-type resonant mode are shown and (b) Phase angle ($\approx \tan^{-1}(Im(\tilde{E})/Re(\tilde{E}))$) of MW Ẽ-field.

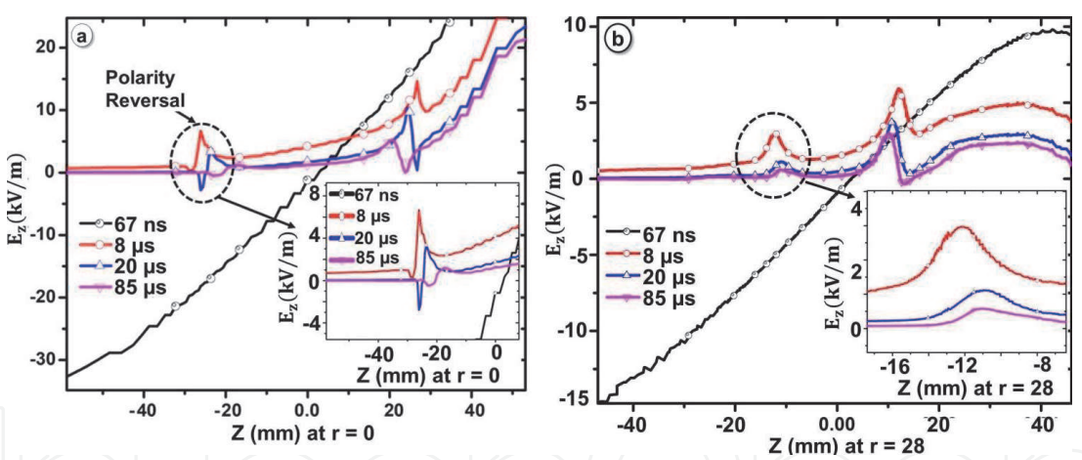

Figure 10.
*Spatio-temporal evolution of E_z-field profile obtained along the axis of the cylindrical cavity. A sharp change in the two places for both the figures implies the power absorption locations that can be checked with **Figure** 5 described above. (a) r = 0 mm, (b) r = 28 mm.*

barrier, it is capable of penetrating the core dense plasma and transferring the energy through damping to the plasma particles. As demonstrated by other groups [23, 28], this change in the power coupling mode from the electromagnetic to electrostatic case is a signature of the UHR heating. Due to the heating at UHR, the plasma electron temperature and also the density are possible to enhance further.

It can be observed in **Figure 8** that the magnitude of the E_r-field at time t = 67 ns (**Figure 8**) is greater than 7 kV/m along different z-planes within the cavity near the ECR locations. This intensity is sufficient for creating ionization in the Argon gaseous particles. In the later instant (~2 μs) of time, the magnitude of E_r-field changes in between 3.75 kV/m and 0.15 kV/m on the ECR regions. This type of nonlinearity in the E_r-field has also been demonstrated by Hopwood et al. [4] before. The power coupling phenomena involved during the plasma evolution can

also be transmitted into the extracted ion beam performance in terms of spike or instabilities. It was experimentally demonstrated by Ropponen et al. [1] that a sharp transient in the ion current density during the preglow mode can cause a sharp fall in the high energy component of the plasma electron temperature.

Since the inhomogeneous part of E_r-field is shifting toward the off-resonance locations as shown in **Figure 8(b)**, it can also produce high-energy electrons there if certain conditions are satisfied as per Gammino et al. [34]. The conditions say the MW electric field has to be above a certain transition value for being capable to energize the electrons that also depend on the magnetic field gradient present in the same location.

The generated high-energy electrons can interact with the slow extraordinary-type microwave and produce the cyclotron range instability in the plasma [1]. It was also proved experimentally by Mansfeld et al. [35] that the extracted ion beam current from the microwave ion source can gain oscillation due to the presence of cyclotron-type instability of plasma during the afterglow operation mode. The slow extraordinary mode microwave is produced from the mode conversion of ordinary-type microwave near the UHR region. As the mode conversion layer is present in the present plasma cavity, the ordinary mode microwave crosses the evanescent layer and some part of its energy is converted into the slow X mode. Since the plasma is confined in the cavity under mirror magnetic field configuration, the injected MW will have two components, extraordinary mode and ordinary mode. **Figure 9(a)** shows the MW ordinary mode is propagating toward the overdense plasma region from the underdense launching point. At some point, it will encounter a cut-off corresponding to the ordinary-type MW. At the cut-off, some part of the ordinary mode MW energy is evanescently transformed into a slow extraordinary mode following the CMA diagram concepts. For that reason, a bend in the MW propagation in the slow extraordinary (X) mode is seen in the electric field simulation (**Figure 9b**). This slow X mode then propagates toward the UHR region and hence the electric field is being accumulated there, as shown in **Figure 9(a)**. The accumulation of the electric field at this location increases its intensity at some plasma condition and can cross the corresponding parametric decay threshold condition. The parametric decay of the slow X mode near the UHR region can generate ion- and electron-type electrostatic waves as per the literature [36].

As a supportive evidence of the generation of electrostatic ion wave, **Figure 8(b)** shows that the inhomogeneous part of the E_r-field is shifting toward the off-resonance region with a velocity of 1250–1500 m/s. This range of velocities falls in the range of ion acoustic speed. Based on the published reports [37], the electric field propagating perpendicularly with respect to the external magnetic field as in the present case (**Figure 9a**) encounters the UHR layer in the overdense plasma state. In the present computation, the ordinary mode (O mode) electric field after converting into the slow extraordinary mode (X mode) shows a bending in the perpendicular direction and reaches the UHR region. This is known as 'O – slow X' conversion process that is responsible for generating ion waves and makes the inhomogeneous electric field to shift at the same ion acoustic speed [38].

4.4 E_z-field evolution in plasma with time

The spatio-temporal evolution of the axial component (E_z) of the electric field is shown in **Figure 10** throughout the cylindrical cavity along the planes r = 0 mm and 28 mm, respectively. It is seen that only a portion of single wavelength of the wave electric field is present that has significant intensity throughout the plasma cavity after the immediate instant (67 ns) of MW launching. The magnitude of the E_z field becomes almost zero throughout the cavity as soon as the plasma starts creating

after the MW launching. Therefore, the E_z field does not play any significant role in accelerating the electrons, and if this would happen, the electrons losses will occur in the axial direction. **Figure 10(a–b)** evidences that the E_z field becomes almost zero everywhere except near the ECR surface after ~8 μs. The E_z-field magnitude shows minimum values where the plasma density is of maximum values.

It can be observed in **Figure 10(a)** that the polarity in the inhomogeneous part of the electric field is getting opposite for two different time instances, 20 and 85 μs. The reversal in the polarity of electric field occurs near the ECR surface. The polarity reversal is caused by the ambipolar field produced from the plasma density gradient. The plasma density gradient is computed from the electron momentum equation using drift-diffusion approach in the present FEM model [38]. The shifting of the inhomogeneous part of the electric field is in the inward direction. The speed of displacement of the inhomogeneous part of the electric field is estimated in the range of $\sim 10^3$ m/s that lies in the range of ion sound speed. Similar shifting at the same velocity is also observed before in **Figure 8**(b) corresponding to the E_r-plots. These observations indicate that the plasma density gradient near the ECR surface is accompanied by the generation of ion acoustic waves that are electrostatic in nature [39, 40]. Hence, the electric field polarity reversal associated with electrostatic ion wave heating is being initiated during this period of the plasma evolution after the microwave launch.

5. Validation with experiment

Experiments are performed to cross-check the above-mentioned plasma parameters obtained during the gas ignition moment. The present section of the chapter provides the details of the experimental methods, analysis of the experimental results and also a comparative study of the experimental data with the simulation.

5.1 Methods of experiment

Experiments are carried out in a microwave ion source system that has similar system configuration, magnetic field distribution, MW conditions and also the operating conditions. The simulated temporal plasma parameters, such as the plasma density and hot electron temperature, are validated with the experiment [23]. In the present experiment, MW-plasma reactor of the experimental set-up is a cylindrical cavity (**Figure 11**) of 107-mm length and 88-mm diameter. The plasma in the reactor is generated by coupling microwave through the electron cyclotron resonance (ECR) heating as well as off-ECR heating methods, as discussed before. The complete experimental set-up consists of a cylindrical cavity, microwave system, ion beam extraction system and two pairs of ring magnets (each magnet has pole strength ~1.38 T) assembly [23]. The plasma cavity/reactor is surrounded by two pairs of ring magnets to generate a mirror-type magnetic field to confine the plasma inside the cavity.

To generate plasma, the MW is produced by a magnetron (power: 0–2 kW, make: Richardson Electronics, Model no. NL10250-7), which is operated either in continuous or in pulsed mode. MW power is fed to the reactor through a combination of a four-step ridged waveguide, a HV break and vacuum window assembly, an impedance tuner unit, directional coupler and an isolator with water dummy load (**Figure 11**). The plasma impedance is matched by a 3-stub tuner to get maximum $\tilde{E}$-field at the center of the MW-plasma reactor. MW is coupled to the cylindrical plasma reactor by a four-step ridged waveguide (WR 284) [23]. The

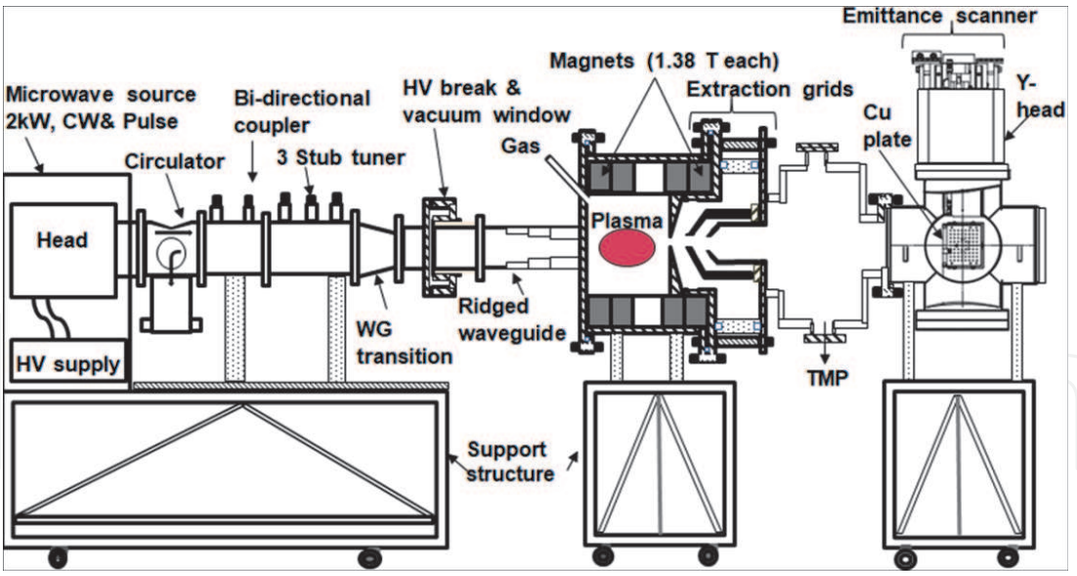

Figure 11.
Schematic view of the experimental system.

impedance of WR284 waveguide (four-step ridge waveguide) having 220-mm length is made comparable to the typical plasma impedance by embedding four ridge sections on both the inner side walls of it. The ridge sections of different lengths but same width (48 mm) are placed consecutively at the broader walls of the waveguide. As shown in **Figure 11**, the ridge waveguide is mechanically connected to one side of a high voltage (HV) break cum vacuum window, made of Teflon having a dimension of 35 mm diameter and 6 mm thickness, whose other side is connected to the ion source cavity (**Figure 11**). The other side of the cavity is connected to the conventional pierce geometry-based 3-grid extraction system, housed in a drift duct vacuum chamber that consists of a plasma grid, an extraction grid and a grounded grid (**Figure 11**). The ion source is evacuated by a combination of Turbo Molecular Pump, which is backed by a dry-scroll rotary pump, connected to the drift duct vacuum chamber in the downstream side of the extraction system. The gas feed system comprises a needle valve, mass flow controller and the required gas cylinder. In the present experiment, nitrogen gas is used because of availability. Other gases, like argon or hydrogen, can also be used. The experiment is carried out for the MW power in the range of 50–700 W and gas pressure in the range of 1×10^{-3} mbar to 1×10^{-4} mbar. The Langmuir probe (LP) diagnostics is used to characterize the plasma parameters within the pressure range varying from 2×10^{-4} to 1×10^{-3} mbar [23].

All the MW power ranges mentioned throughout the chapter are considered as set power. The difference of forward and reflected power is considered to be plasma-absorbed power. MW reflection varies from 5 to 10% within the above set power range. These ranges of plasma reflection with similar experimental set-ups and operating environments are reported in [10]. The accuracy at low set power levels of magnetron is tested by repeated measurements of its output power (forward) before the experiment is performed. An extra component, named isolator with water-cooled dummy load (make: National Electronics, Model: 2722-162-10311, isolation: 26 dB, reflection rating: 6.5 kW) is placed in the experimental set-up (not shown in **Figure 11**) before the HV break. The power and carrier frequency signals are measured by microwave spectrum analyzer (model: FSH8, make: ROHDE & SCHWARZ, band: 100 Hz–8 GHz) at the directional coupler port. Signals are attenuated by 60 dB ($\equiv 10^6$, power ratio) at the directional coupler ports

before coming to microwave spectrum analyzer through the high frequency (0–40 GHz), low loss and low VSWR cable of length ~1 m.

To generate plasma in the low power range, magnetron's low power testing is required. In the present experiment, low power testing ensures the variation of full width at half maximum of 2.45 GHz frequency is within 5–12 MHz (within the specified ± 25 MHz bandwidth as per Sairem data). Also, the set power fluctuations are within 2–5% as shown in **Figure 12(a)**, which is considered to be stable operating conditions. After performing the inverse Fourier transform of the MW spectrum analyzer data, a graph of detected MW power vs. time is shown in **Figure 12 (b)** to verify the power levels at the first few milliseconds for the comparison of plasma parameters with the simulated data. The rise time of the pulse is obtained as ~2.2 μs.

The magnetron's output (set power) in the low power range is checked in time scale prior to the Langmuir probe diagnostic [23]. The response of the magnetron set power at 2.45 GHz frequency is recorded at the directional coupler port by a microwave spectrum analyzer (SA) circuitry. The circuitry consists of a high frequency cable, a band pass filter, and spectrum analyzer and FSH4 View software.

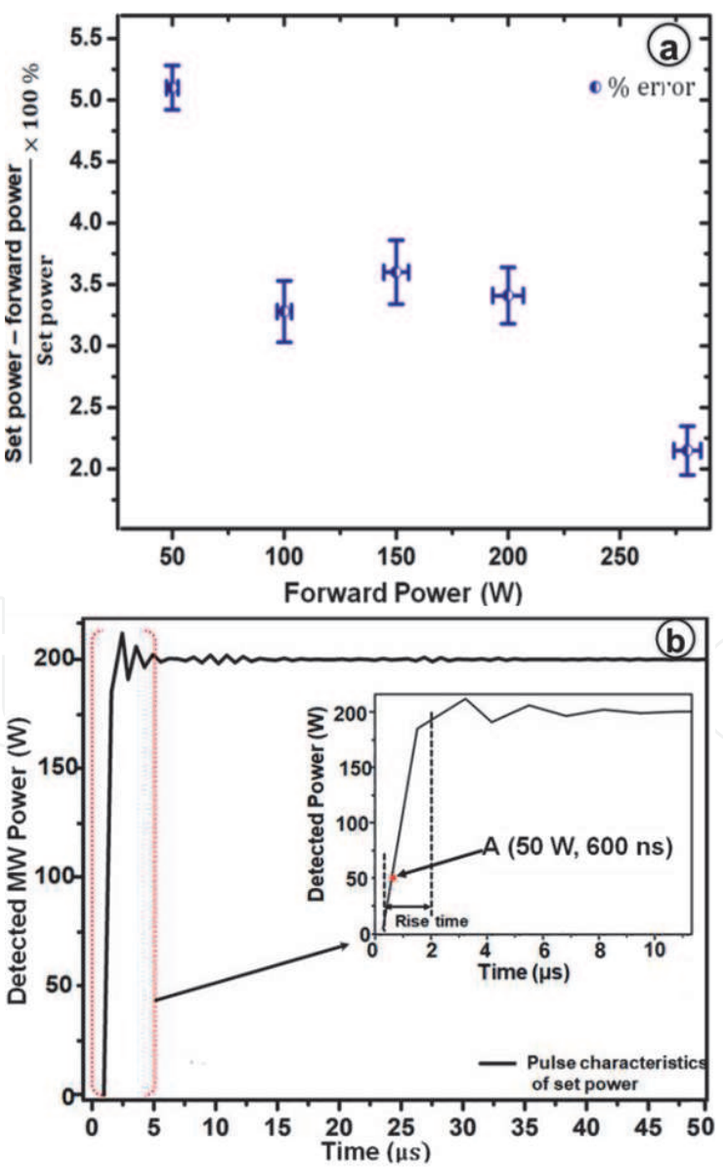

Figure 12.
(a) Percentage error of the magnetron set power fluctuations. Data for 280 W have been benchmarked with the Sairem company data and (b) variation of the detected MW power vs. time for the set power of 200 W.

The magnetron's pulse response at a fixed set power, 200 W, is obtained by taking the inverse Fourier transform of the microwave spectrum analyzer data. The magnetron's rise time is ~2.2 μs. This exercise of measuring the pulse response of a particular set power can help to pick up the temporal values at different set power levels following the pulse response of magnetron [23].

To compare the simulated hot electron temperature and density, their parameters are noted down at different instant of time during the plasma evolution. Taking the time instant to be same as that of the simulation, the set power values are noted down in an experimental datasheet. Then, a single Langmuir probe measures the plasma floating potential at the noted set power values as mentioned above [23]. The Langmuir probe measurement is performed in steady state plasma condition. Since the real-time measurement of the plasma parameter requires in the ns-time scale very sophisticated and expensive hardware that has faster time responses (ns range), steady state Langmuir probe measurements are performed to avoid those expensive diagnostics.

5.2 Comparison of experimental results with simulation

The line plots are shown in **Figure 13(a)** for the simulated hot T_e. The simulated data point lies in a region that is very close to the experimental data points. The simulated hot T_e is approximately 78 eV at 70 W of plasma absorbed power during time t = 600 ns. One can also observe that the set power for the magnetron reaches 50 W at the same time instant. The measurement of the hot T_e by a Langmuir probe diagnostic at the same set power level shows it to be ~ 72 eV. Similarly, the hot T_e was measured for two other power levels, 70 and 130 W. The hot T_e at these two power levels are ~ 36 and 28 eV, respectively. Hence, the experimental results fit well with the simulated values described above [23]. On the other hand, the experimental data for the plasma density are also shown in **Figure 13(b)**. The plasma densities for the above set power levels are observed to be ~1.8–2 times less than the simulated data. The deviation of the measured plasma density from the simulated values is caused due to the difference in the absorbed power that is absorbed by the plasma in both the cases (experiment and simulation). The experimental results for the plasma density are shown in **Figure 13(b)** for three different set powers. The measured plasma density ($\sim 1.1 \times 10^{17} m^{-3}$) at set power of 200 W agrees well with the simulated plasma density ($\sim 1.3 \times 10^{17} m^{-3}$).

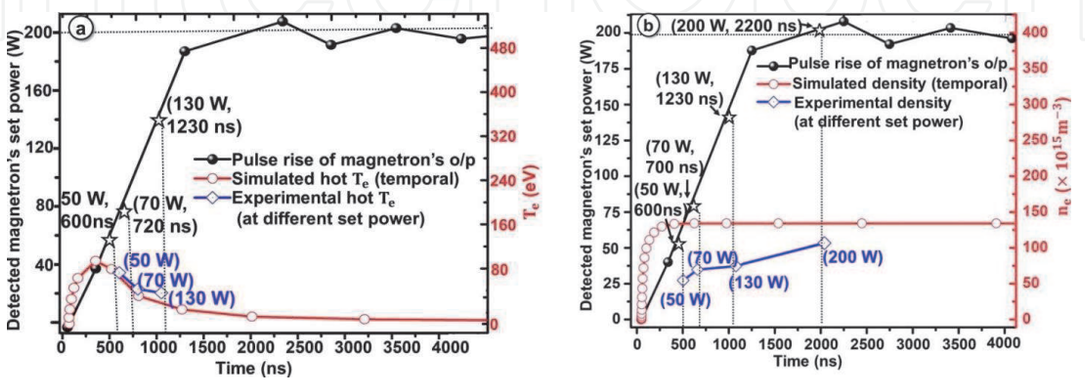

Figure 13.
(a) Simulated temporal hot T_e variation along with experimental data, taken at discrete set power values. Plasma-absorbed power during simulated hot T_e evolution is fixed at 70 W. Experimental set powers 50, 70 and 130 W correspond to plasma-absorbed powers at 40, 50 and 70 W, respectively [14]. Pulse rise of set power is also shown to verify the power levels during the ns to few μs periods. (b) Simulated temporal plasma density variation along with experimental results, obtained at the same set power values.

6. Conclusion

The evolution of the spatial and temporal plasma parameters are presented in the current chapter during the gas ignition process made by injecting the 2.45 GHz microwave to an ion source cavity. The simulated results supported by the experiment confirm that the plasma parameters are influenced significantly by the electric fields during the plasma ignition period. Due to the shifting of the microwave coupling mechanisms to the plasma, the plasma density and the hot fraction of the electron temperature are also getting affected during the plasma generation period. The initial rise of the hot fraction of the plasma electron temperature from the start of microwave interaction into the plasma is argued to be caused by the electron cyclotron resonance heating phenomenon. After certain instant of microwave launch, the slight increase in the plasma density and the decrease in the plasma electron temperature are proved to be happening from the electrostatic heating mechanism. The electrostatic heating near the upper hybrid resonance region causes to shift the inhomogeneous part of the electric field at the velocity of the ion acoustic speed when the plasma density reaches above the critical density corresponding to the launch microwave, 2.45 GHz.

The experimental plasma parameters are obtained in an experimental set-up that has similar system configuration and the operating environment as that of the simulation. The comparison shows a reasonable agreement with the simulated results. The plasma density especially in the overdense plasma condition is found to be agreeing more in the overdense plasma than in the underdense plasma condition. During plasma evolution after the microwave launch, the microwave coupling mechanisms are modified following the corresponding electric field (electrostatic and electromagnetic) distribution pattern throughout the ion source cavity. Initially, the electron cyclotron resonance heating comes into play to ionize the gaseous particle and generate plasma that contains the maximum fraction of the high-energy electrons in the ion source plasma. Then, as the density reaches in the overdense condition, the coupling mechanisms are the electrostatic wave heating in the ion acoustic frequency range. As the electrostatic wave does not suffer any density cut-off, the density is increased further above the critical density. Simultaneously, the polarity of the axial electric field is reversed near the electron cyclotron resonance region signifying the creation of the plasma density gradient due to the generation of strong ambipolar electric field near the resonance region. In future, it is intended to study the different power coupling mechanisms in the overdense plasma state that are caused due to the heating at the cyclotron harmonics by the generated electrostatic waves in the present experimental device.

Author details

Chinmoy Mallick[1,2*], Mainak Bandyopadhyay[1,2] and Rajesh Kumar[1,2]

1 Institute for Plasma Research (IPR), Gandhinagar, Gujarat, India

2 Homi Bhabha National Institute (HBNI), Mumbai, Maharashtra, India

*Address all correspondence to: chinmoyju1990@gmail.com

References

[1] Ropponen T, Tarvainen O, Izotov I, Noland J, Toivanen V, Machicoan G, et al. Studies of plasma breakdown and electron heating on a 14 GHz ECR ion source through measurement of plasma bremsstrahlung. Plasma Sources Science and Technology. 2011;**20**:055007. DOI: 10.1088/0963-0252/20/5/055007

[2] Cortázar OD, Megía-Macías A, Vizcaíno-de-Julián A. Experimental study of breakdown time in a pulsed 2.45-GHz ECR hydrogen plasma reactor. IEEE Transactions on Plasma Science. 2012;**40**:3409. DOI: 10.1063/1.4819875

[3] Cortazar OD, Megía-Macías A, Tarvainen O, Vizcaíno-de-Julián A, Koivisto H. Plasma distributions observed in a 2.45 GHz hydrogen discharge. Plasma Sources Science and Technology. 2014;**23**:065028. DOI: 10.1088/0963-0252/23/6/065028

[4] Hopwood J, Wagner R, Reinhard DK, Asmussen J. Electric fields in a microwave-cavity electron-cyclotron-resonant plasma source. Journal of Vacuum Science and Technology A. 1990;**8**:2904. DOI: 10.1116/1.576647

[5] Stenzel RL. A new probe for measuring small electric fields in plasmas. The Review of Scientific Instruments. 1991;**62**:130. DOI: 10.1063/1.1142514

[6] Celona L, Gammino S, Ciavola G, Maimone F, Mascali D. Microwave to plasma coupling in electron cyclotron resonance and microwave ion sources. Review of Scientific Instruments. 2010; **81**:02A333. DOI: 10.1063/1.3265366

[7] Consoli F, Celona L, Ciavola G, Gammino S, Maimone F, Barbarino S, et al. Influence of microwave driver coupling design on plasma density at Test-bench for Ion sources Plasma Studies, a 2.45 GHz electron cyclotron resonance plasma reactor. Review of Scientific Instruments. 2008;**79**:02A308. DOI: 10.1063/1.2805665

[8] Takahashi K, Kaneko T, Hatakeyama R. Polarization-reversal-induced damping of left-hand polarized wave on electron cyclotron resonance. Physical Review Letters. 2005;**94**: 215001. DOI: 10.1103/PhysRevLett.94.215001

[9] Becker MM, Kählert H, Sun A, Bonitz M, Loffhagen D. Advanced fluid modeling and PIC/MCC simulations of low-pressure ccrf discharges. Plasma Sources Science and Technology. 2017; **26**:044001. DOI: 10.1088/1361-6595/aa5cce

[10] Hagelaar GJM, Makasheva K, Garrigues L, Boeuf JP. Modelling of a dipolar microwave plasma sustained by electron cyclotron resonance. Journal of Physics D: Applied Physics. 2009;**42**: 194019. DOI: 10.1088/0022-3727/42/19/194019

[11] COMSOL Multiphysics Reference Manual, Version 5.2. COMSOL, Inc. Available from: www.comsol.com

[12] Eric J. Vanzura et al, The NIST 60 Millimeter Diameters Cylindrical Cavity Resonator: Performance Evaluation for Permittivity Measurements', NIST Technical Note 1354. 1993

[13] Celona L et al. Observations of resonant modes formation in microwave generated magnetized plasmas. European Physical Journal D: Atomic, Molecular, Optical and Plasma Physics. 2011;**61**:107-115

[14] McDonald KT. An Electrostatic Wave. arXiv:physics/0312025

[15] Chen FF. Introduction to the Plasma Physics and Controlled Fusion: Plasma

Physics. UK: London Press, London; 1986. Addison-Wesley; 1994

[16] Muller A et al. On the charge state distribution of multiply charged ions extracted from electron beam ion sources. Nuclear Instruments and Methods. 1977;**140**:181

[17] Stix TA. Waves in Plasmas. New York: Springer-Verlag; 1992

[18] Mascali D. A new approach to the study of the ECR heating and particle dynamics in the plasma of electron cyclotron ion sources [PhD thesis]. UniversitA degli studi di Catania; 2008

[19] Castro G et al. Study of innovative plasma heating methods and applications to high current ion sources [PhD thesis]. Universita degli Studi di Catania;

[20] Castro G et al. Experimental investigation of non-linear wave to plasma interaction in a quasi-flat magnetostatic field. Review of Scientific Instruments. 2016;**87**:02A507

[21] Stix TH, Swanson DG. Propagation and mode conversion for waves in non-uniform plasmas. In: Galeev A, Sudan RN, editors. Plasma Physics Lab. Rep. PPPL-1903 (June 1982); Handbook of Plasma Physics. Vol. 1. North Holland, Amsterdam: Princeton University; (to be published)

[22] Mallick C, Bandyopadhyay M, Kumar R. Spatio-temporal evolution of electric field inside a microwave discharge plasma during initial phase of ignition and its effect on power coupling. Physics of Plasmas. 2019;**26**: 043507. DOI: 10.1063/1.5085204

[23] Mallick C, Bandyopadhyay M, Kumar R. Plasma characterization of a microwave discharge ion source with mirror magnetic field configuration. The Review of Scientific Instruments. 2018;**89**:125112. DOI: 10.1063/1.5048292

[24] Kinder RL, Kushner MJ. Wave propagation and power deposition in magnetically enhanced inductively coupled and helicon plasma sources. Journal of Vacuum Science and Technology A. 1999;**17**:2421. DOI: 10.1116/1.581978

[25] Mascali D, Celona L, Gammino S, Miracoli R, Castro G, Gambino N, et al. Electrostatic wave heating and possible formation of self-generated high electric fields in a magnetized plasma. Nuclear Instruments and Methods in Physics Research A. 2011;**653**:11-16. DOI: 10.1016/j.nima.2011.02.04

[26] You HJ, Meyer FW, Chung KS. The cold and hot electron populations, temperatures and their transports in the edge plasma of the ORNL CAPRICE ECR ion source. Plasma Sources Science and Technology. 2009;**18**: 015004. DOI: 10.1088/0963-0252/18/1/ 015004

[27] Chen L, Zhao Y, Wu K, Wang Q, Meng Y, Ren Z. On the generation of magnetic field enhanced microwave plasma line. Physics of Plasmas. 2016;**23**: 123509. DOI: 10.1063/1.4971446

[28] Mascali D, Celona L, Gammino S, Castro G, Miracoli R, Romano FP, et al. An investigation on the formation of suprathermal electrons in a B-min ECR machine and a novel method for their damping. Plasma Sources Science and Technology. 2013;**22**:065006. DOI: 10.1088/0963-0252/22/6/065006

[29] Sugai H, Ghanashev I, Mizuno K. Transition of electron heating mode in a planar microwave discharge at low pressures. Applied Physics Letters. 2000;**77**:3523. DOI: 10.1063/1.1329322

[30] Shalashov AG, Viktorov ME, Mansfeld DA, Golubev SV. Kinetic instabilities in a mirror-confined plasma sustained by high-power microwave radiation. Physics of Plasmas. 2017;**24**: 032111. DOI: 10.1063/1.4978565

[31] Bodendorfer M, Altwegg K, Wurz P, Shea H. Field structure and electron life times in the MEFISTO electron cyclotron resonance ion source. Nuclear Instruments and Methods in Physics Research B. 2008;**266**:4788. DOI: 10.1016/j.nimb.2008.07.019

[32] Izotov I, Tarvainen O, Mansfeld D, Skalyga V, Koivisto H, Kalvas T, et al. Microwave emission related to cyclotron instabilities in a minimum-B electron cyclotron resonance ion source plasma. Plasma Sources Science and Technology. 2015;**24**:045017. DOI: 10.1088/0963-0252/24/4/045017

[33] Chelvam PP, Raja LL. Modeling of gas breakdown and early transients of plasma evolution in cylindrical all-dielectric resonators. Journal of Physics D: Applied Physics. 2017;**50**:474003. DOI: 10.1088/1361-6463/aa925f

[34] Gammino S, Mascali D, Celona L, Maimone F, Ciavola G. Considerations on the role of the magnetic field gradient in ECR ion sources and build-up of hot electron component. Plasma Sources Science and Technology. 2009; **18**:045016. DOI: 10.1088/0963-0252/18/4/045016

[35] Mansfeld D, Izotov I, Skalyga V, Tarvainen O, Kalvas T, Koivisto H, et al. Dynamic regimes of cyclotron instability in the afterglow mode of minimum-B electron cyclotron resonance ion source plasma. Plasma Physics and Controlled Fusion. 2016;**58**: 045019. DOI: 10.1088/0741-3335/58/4/045019

[36] Castro G, Mascali D, Gammino S, Torrisi G, Romano FP, Celona L, et al. Overdense plasma generation in a compact ion source. Plasma Sources Science and Technology. 2017;**26**: 055019. DOI: 10.1088/1361-6595/aa61c4

[37] Van Niekerk EG, Krumm PH, Alport MJ. Electrostatic ion cyclotron waves driven by a radial electric field. Plasma Physics and Controlled Fusion. 1991;**33**:375-388

[38] Schulze J, Donkó Z, Lafleur T, Wilczek S, Brinkmann RP. Spatio-temporal analysis of the electron power absorption in electropositive capacitive RF plasmas based on moments of the Boltzmann equation. Plasma Sources Science and Technology. 2018;**27**: 055010

[39] Dieckmann ME, Sarri G, Doria D, Ynnerman A, Borghesi M. Particle-in-cell simulation study of a lower-hybrid shock. Physics of Plasmas. 2016;**23**: 062111

[40] Fischer P, Gauthereau C, Godiot J, Matthieussent G. Ion acoustic wave generation by a standing electromagnetic field in a sub-critical plasma. Journal de Physique. 1987;**48**: 233-238